

Different methods to derive the mixing-layer height by remote sensing, including RASS

Stefan Emeis

*Institute for Meteorology and Climate Research
Atmospheric Environmental Research Division (IMK-IFU)
Forschungszentrum Karlsruhe GmbH
Kreuzackbahnstr. 19
82467 Garmisch-Partenkirchen, Germany
E-mail: stefan.emeis@kit.edu*

Introduction

- **relevance of mixing layer**
- **definition of mixing layer**
- **remote sensing**

mixing-layer height is relevant:

- meteorology: upper limit of a (usually) turbulent and well-mixed layer**
- air quality: upper limit to vertical dilution, the mixed-layer underneath is usually more polluted than the free atmosphere above**
- wind and turbulence profiles: one of the scaling lengths**

The vertical wind profile

logarithmic law

(with stability correction) $u(z) = (u_*/\kappa) (\ln(z/z_0) - \psi(z/L_*))$

power law

$$u(z) = u(z_A) (z/z_A)^n$$

New proposal
(Gryning et al. 2007)

$$u(z) = \frac{u_{*0}}{\kappa} \left(\ln \left(\frac{z}{z_0} \right) + \frac{z}{L_{MBL,N}} - \frac{z}{z_i} \left(\frac{z}{2L_{MBL,N}} \right) \right)$$

needs information on the PBL or mixing-layer height



Gryning et al., 2007: On the extension of the wind profile over homogeneous terrain beyond the surface boundary layer. Bound.-Lay. Meteorol., **124**, 251–268.

Mixing-layer height

Inversion height

literally: inversion in the temperature profile, increase of temperature with height, strong decrease of moisture, radiation inversions, sinking inversions, surface inversions, lifted inversions

Mixing-layer height

defined by the turbulence profile, upper boundary for vertical exchange (mixing), upper boundary of the well-mixed layer, entrainment

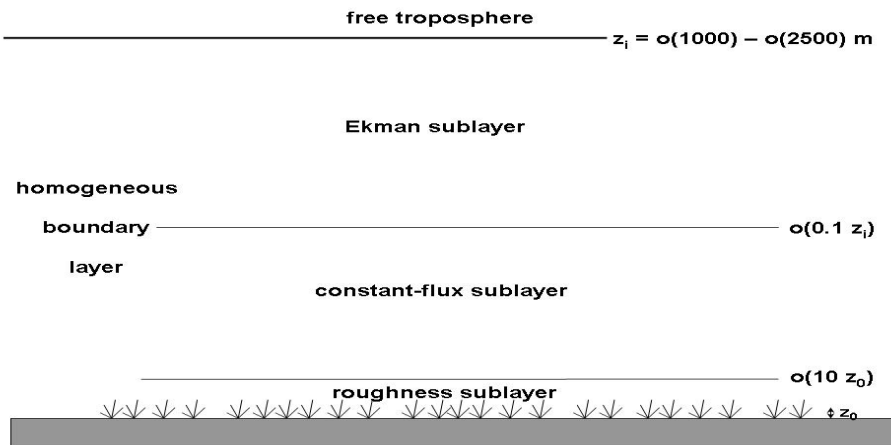
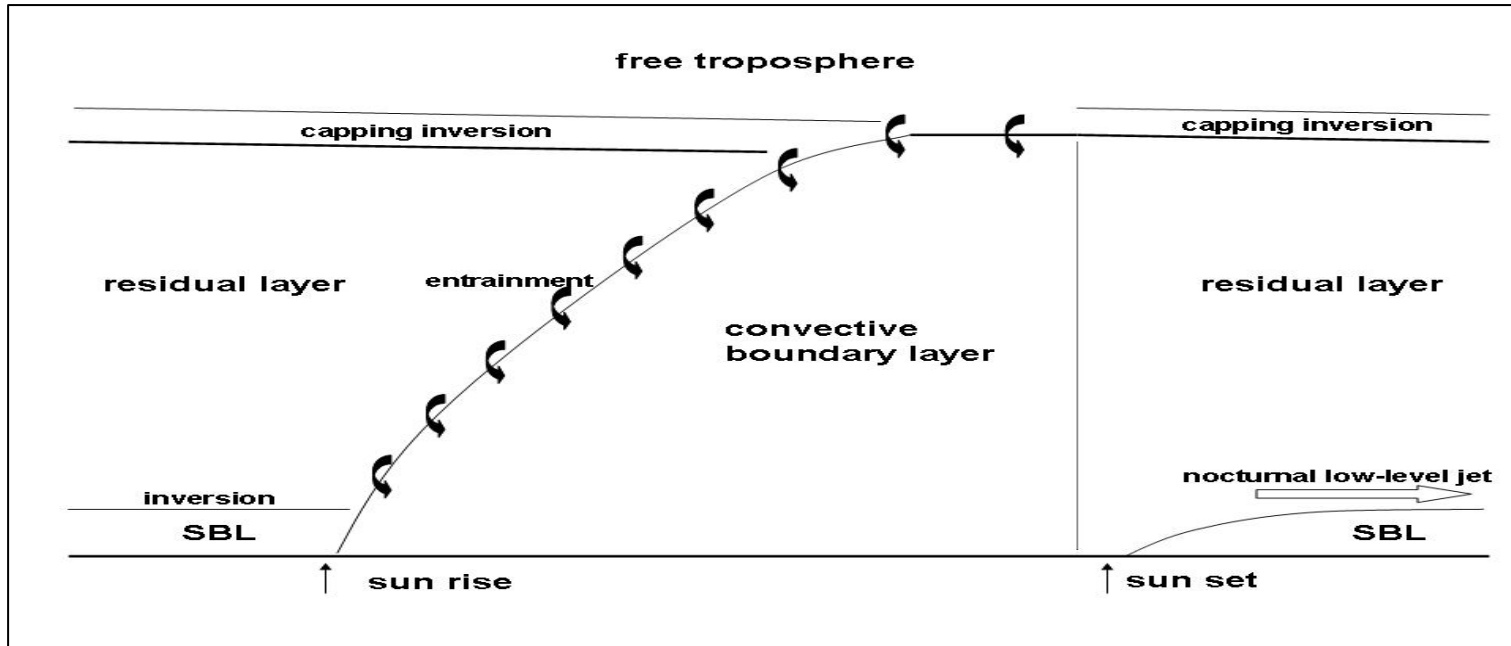
Boundary layer height

SBL: at night, height of the near-surface layer influenced by surface friction
CBL: at day, height of convective plumes

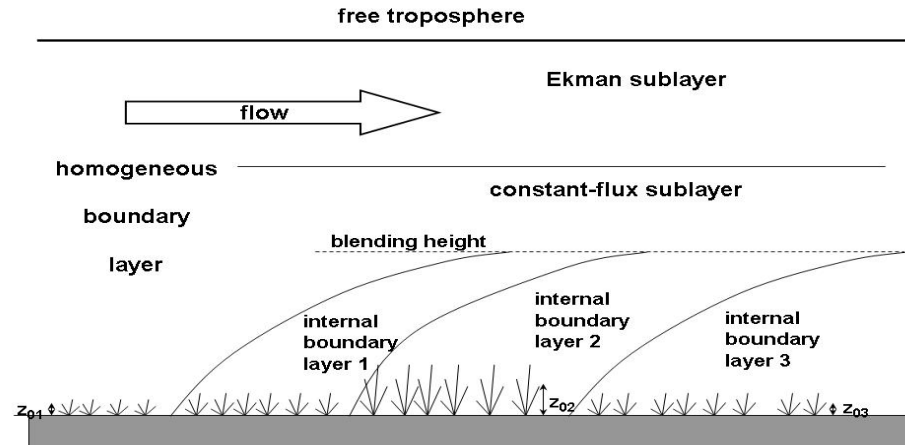
boundary layer height \approx mixing-layer height

boundary layer height \geq inversion height

diurnal variation of PBL

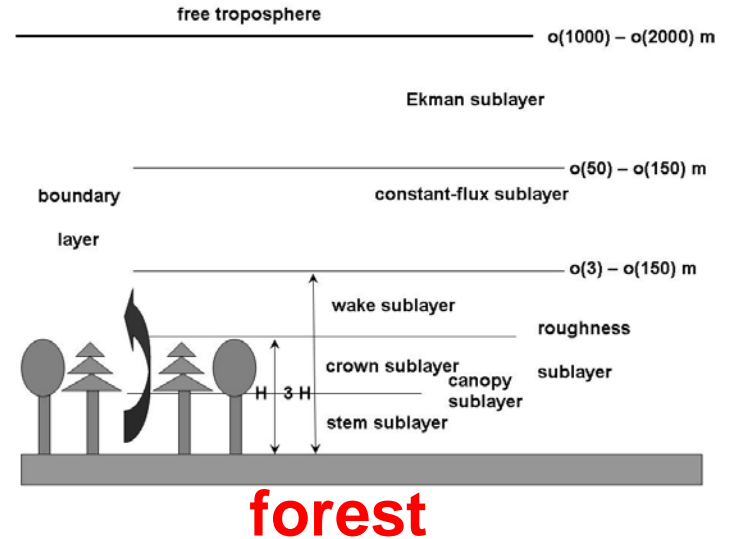
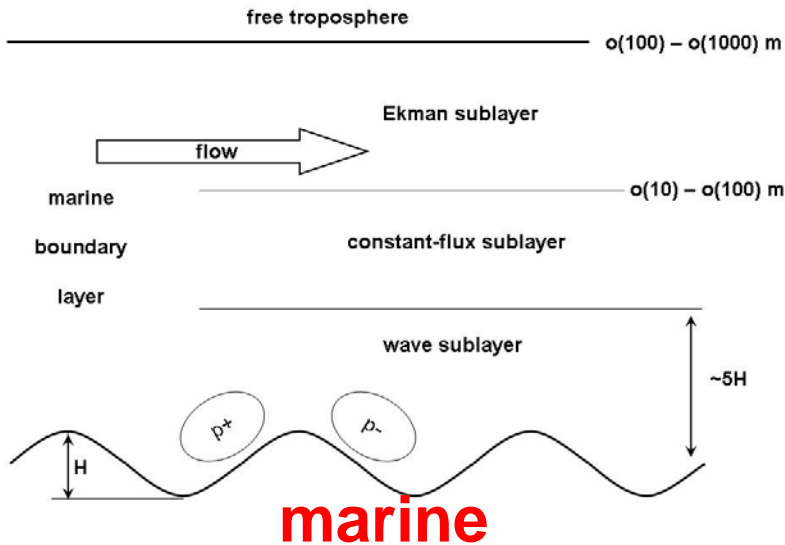
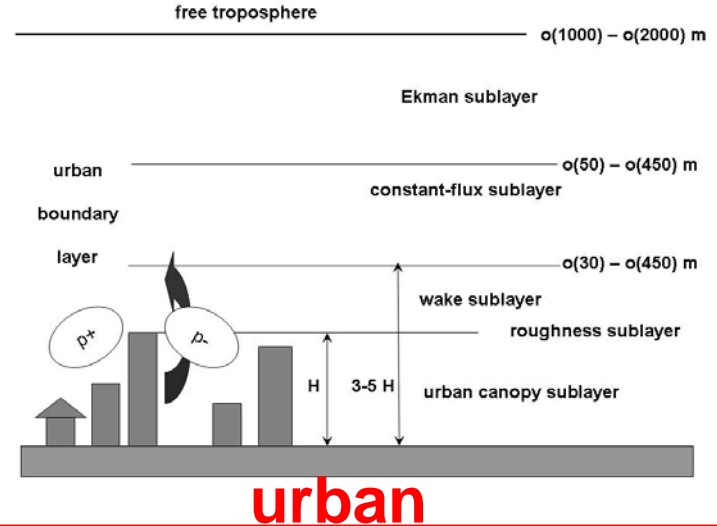
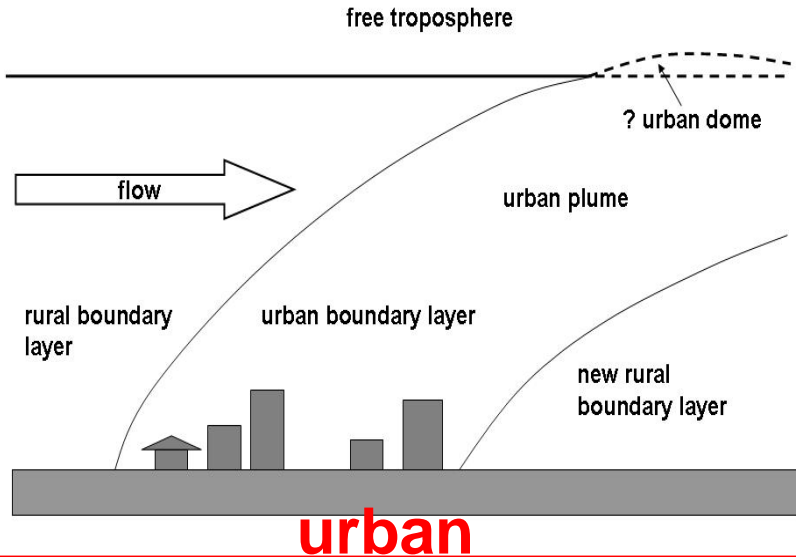


vertical structure of PBL



internal layers in PBL

special types of PBL



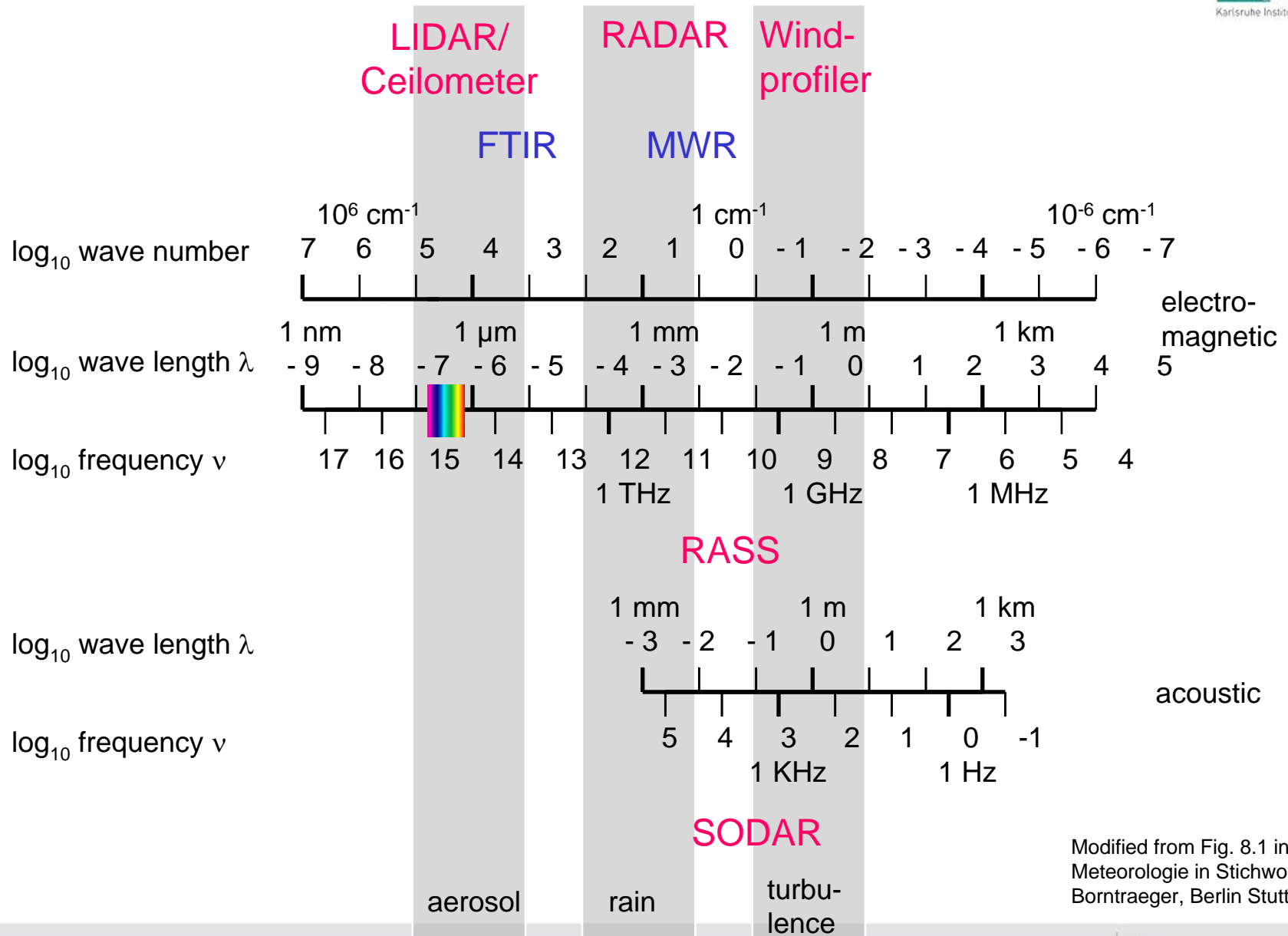
Basic remote sensing techniques

| name | principle | spatial resolution | direction | type |
|------------|--|-------------------------|--|---|
| RADAR | backscatter, electro-magnetic pulses, fixed wave length | profiling | scanning, slanted | active, monostatic |
| SODAR | backscatter, acoustic pulses, fixed wave length | profiling | fixed, slanted, vertical | active, usually monostatic |
| LIDAR | backscatter, optical pulses, fixed wave length(s) | profiling | scanning, fixed, horizontal, slanted, vertical | active, monostatic |
| RASS | backscatter, acoustic, electro-magnetic, fixed wave length | profiling | fixed, vertical | active, monostatic |
| | absorption, infrared, spectrum | path-averaging | fixed, horizontal, slanted | active, bistatic or passive |
| FTIR | emission, infrared, spectrum | path-averaging | fixed, horizontal, slanted | passive |
| DOAS | absorption, optical, fixed wave lengths | path-averaging | fixed, horizontal | active, bistatic |
| radiometry | electro-magnetic, fixed wave length(s) | averaging, profiling | fixed, scanning, slanted, vertical | passive |
| tomography | travel time, acoustic, fixed wave length | horizontal distribution | fixed, horizontal | active, multiple emitters and receivers |

subject of this talk

subject of this talk

Typical frequency bands for remote sensing of the atmosphere

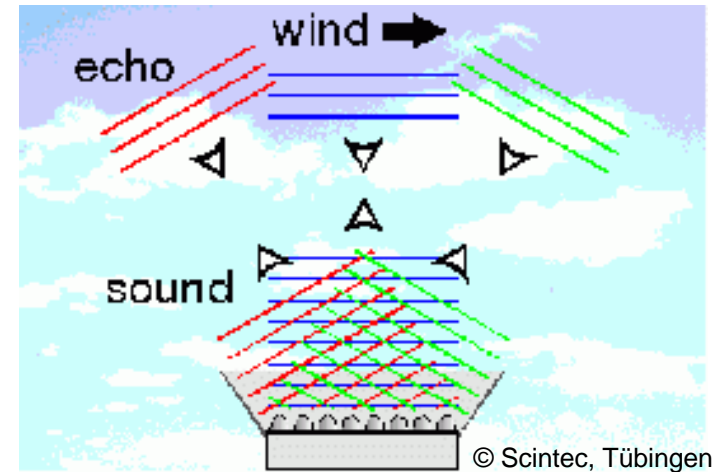
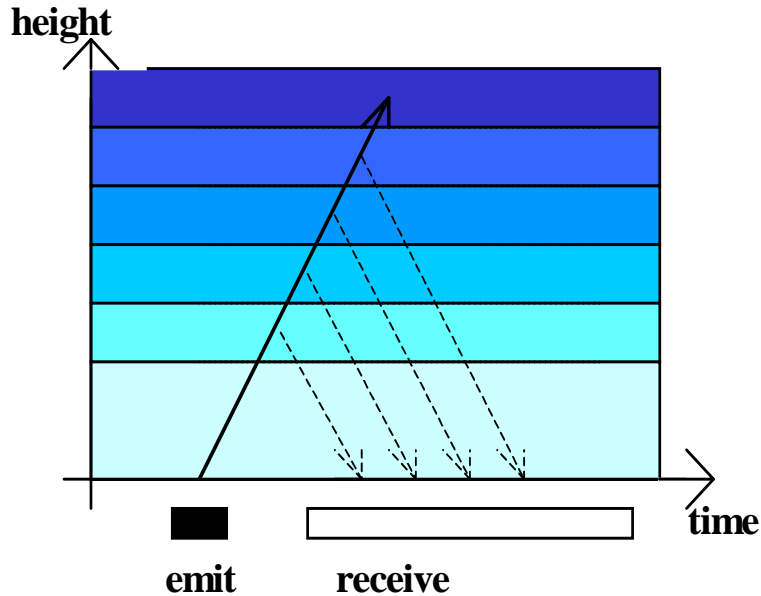


Modified from Fig. 8.1 in „
 Meteorologie in Stichworten“,
 Borntraeger, Berlin Stuttgart 2000

SODAR

algorithms for mixing-layer height

monostatic SODAR: measuring principles



deduction:

| | | |
|-----------------------|---|------------|
| sound travel time | = | height |
| backscatter intensity | = | turbulence |
| Doppler-shift | = | wind speed |

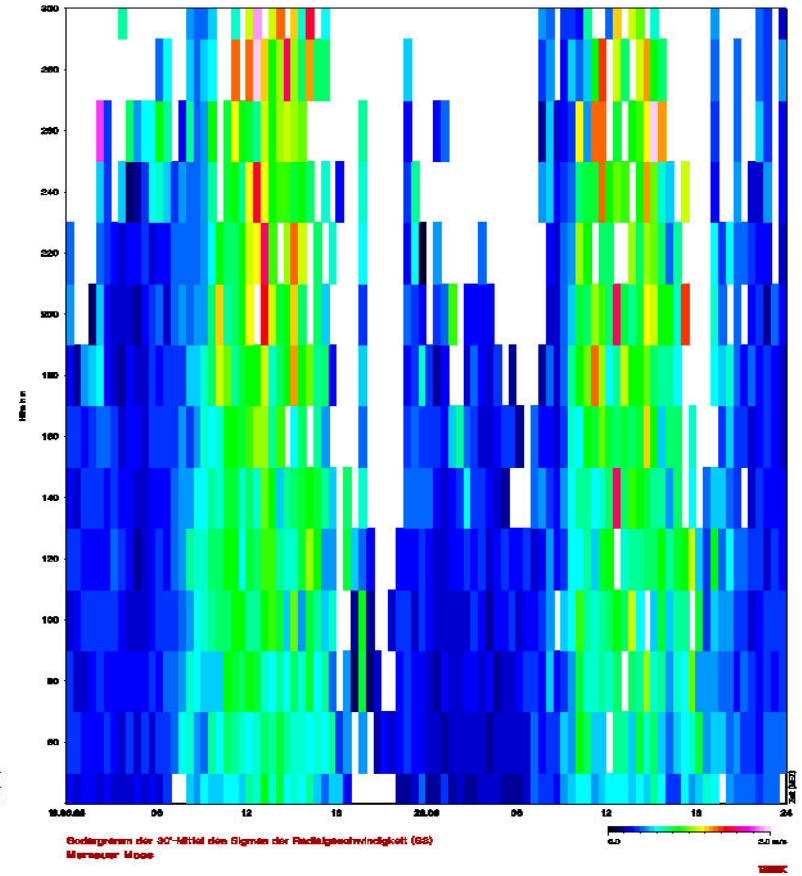
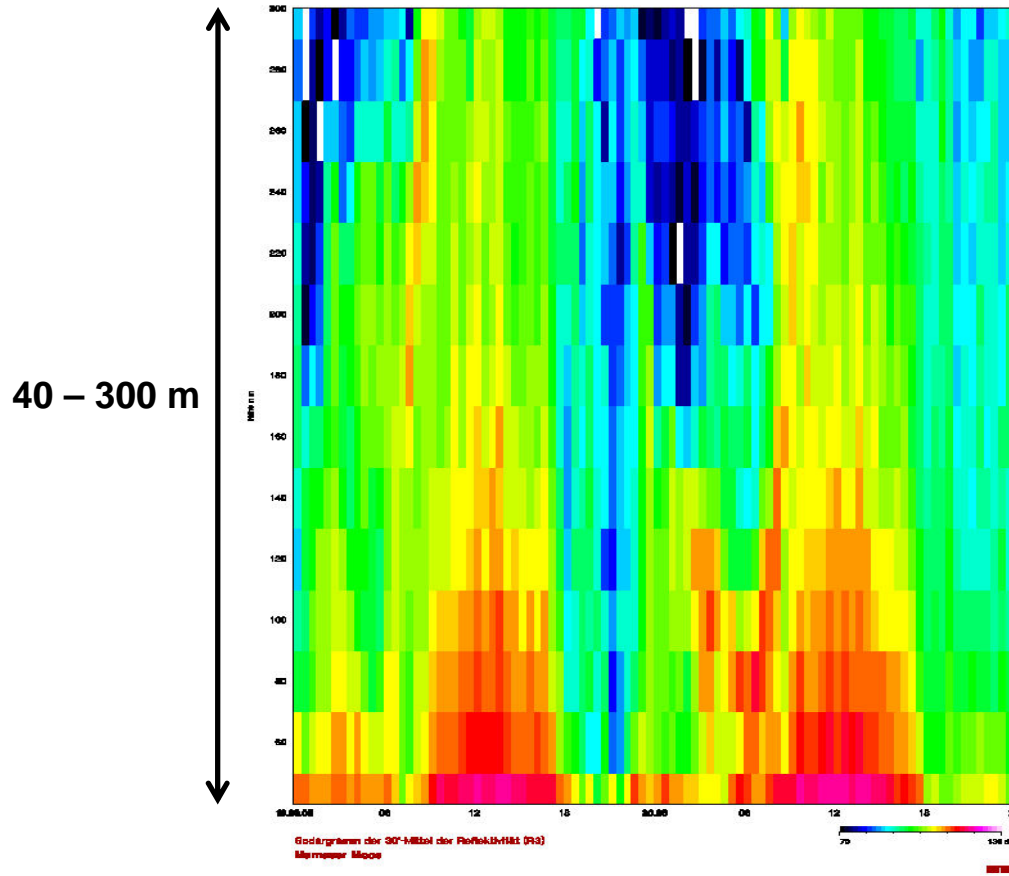
Emission of sound waves
into three directions:

in order to measure all three
components of the wind
(horizontal and vertical)

Sample plot SODAR (convective BL at daytime)

acoustic backscatter intensity

sigma w

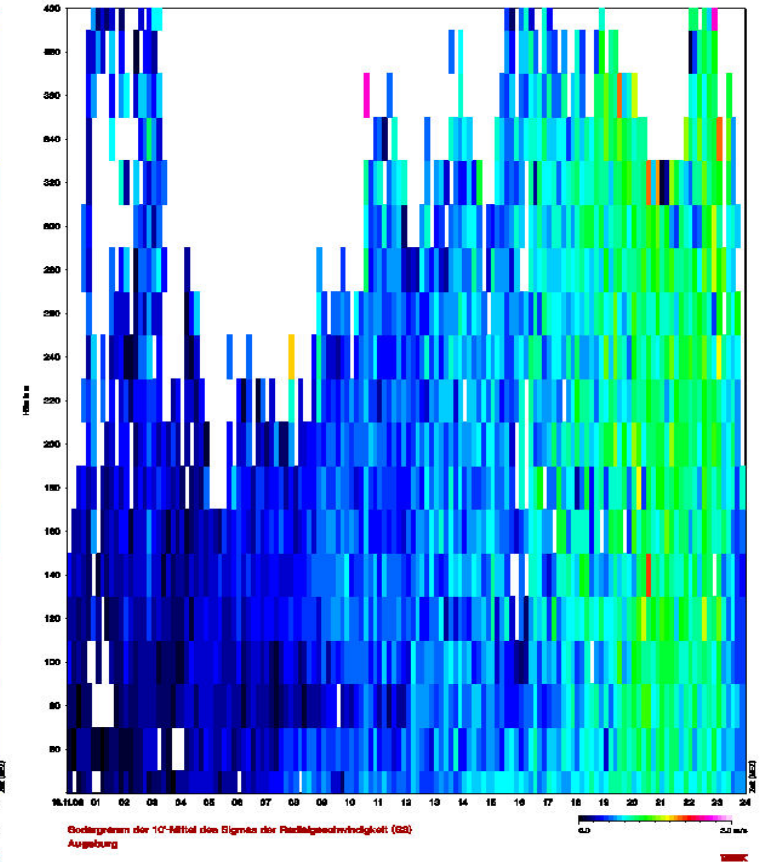
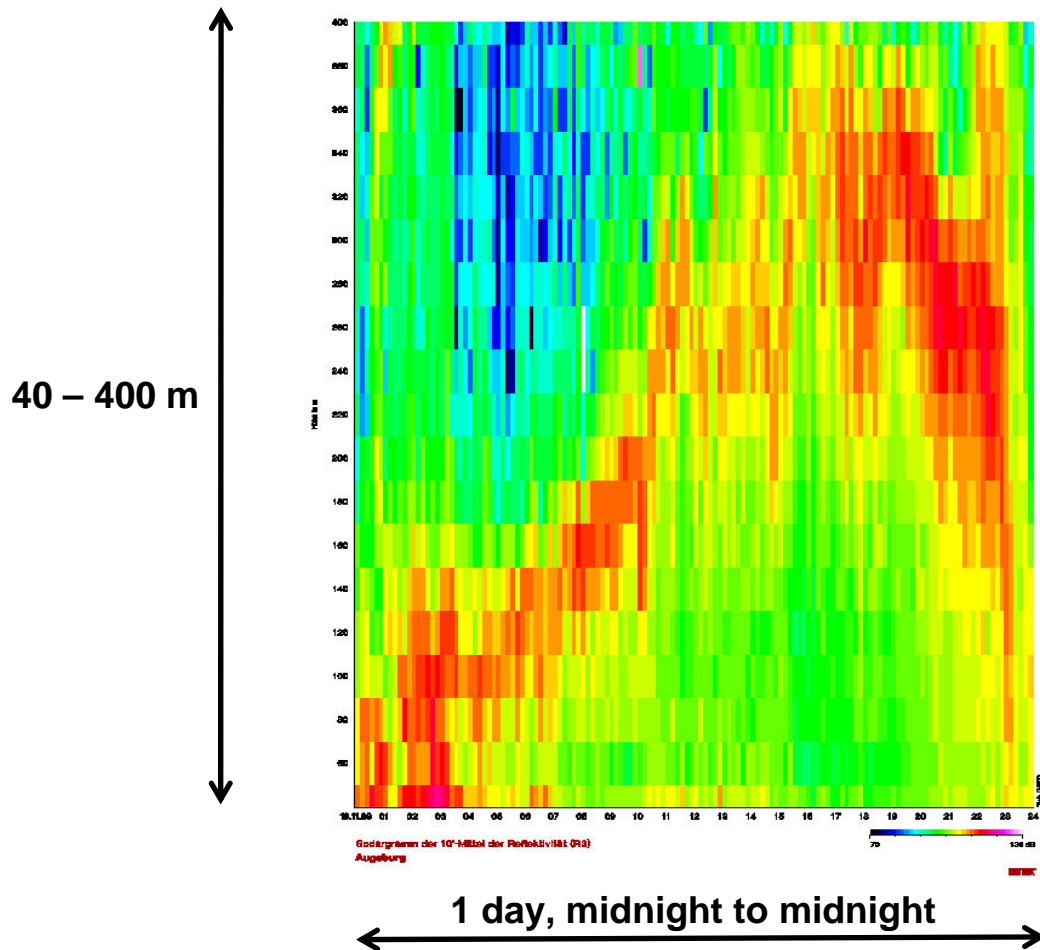


2 days, midnight to midnight

Sample plot SODAR (lifted inversion)

acoustic backscatter intensity

sigma w

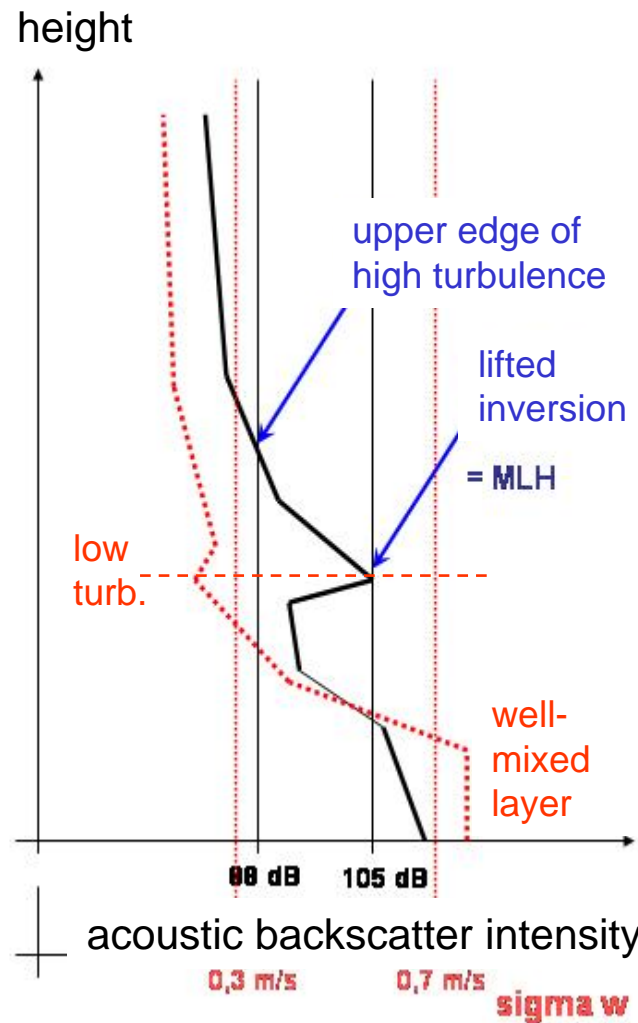


Algorithms to detect MLH from SODAR data

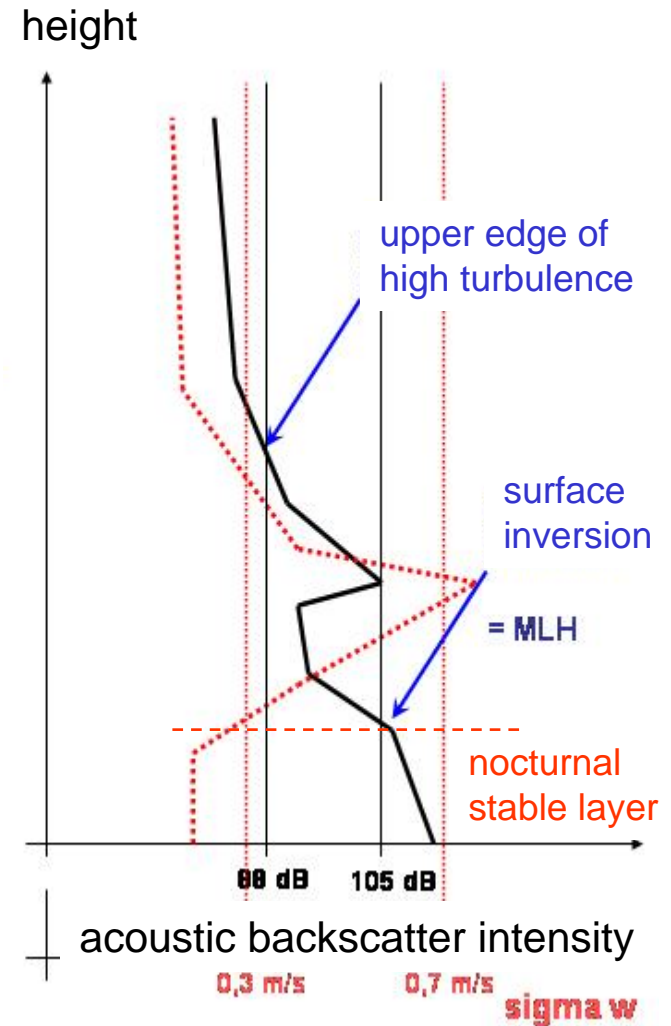
criterion 1:
 upper edge of high turbulence

criterion 2:
 surface and lifted inversions

$$MLH = \text{Min} (C1, C2)$$



example 1: daytime

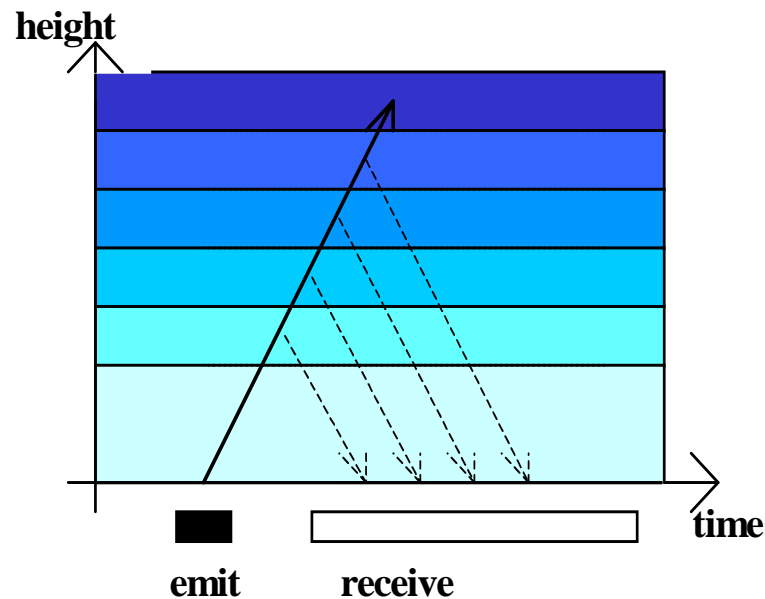


example 2: night-time

Ceilometer

algorithms for mixing-layer height

Ceilometer/LIDAR measuring principle



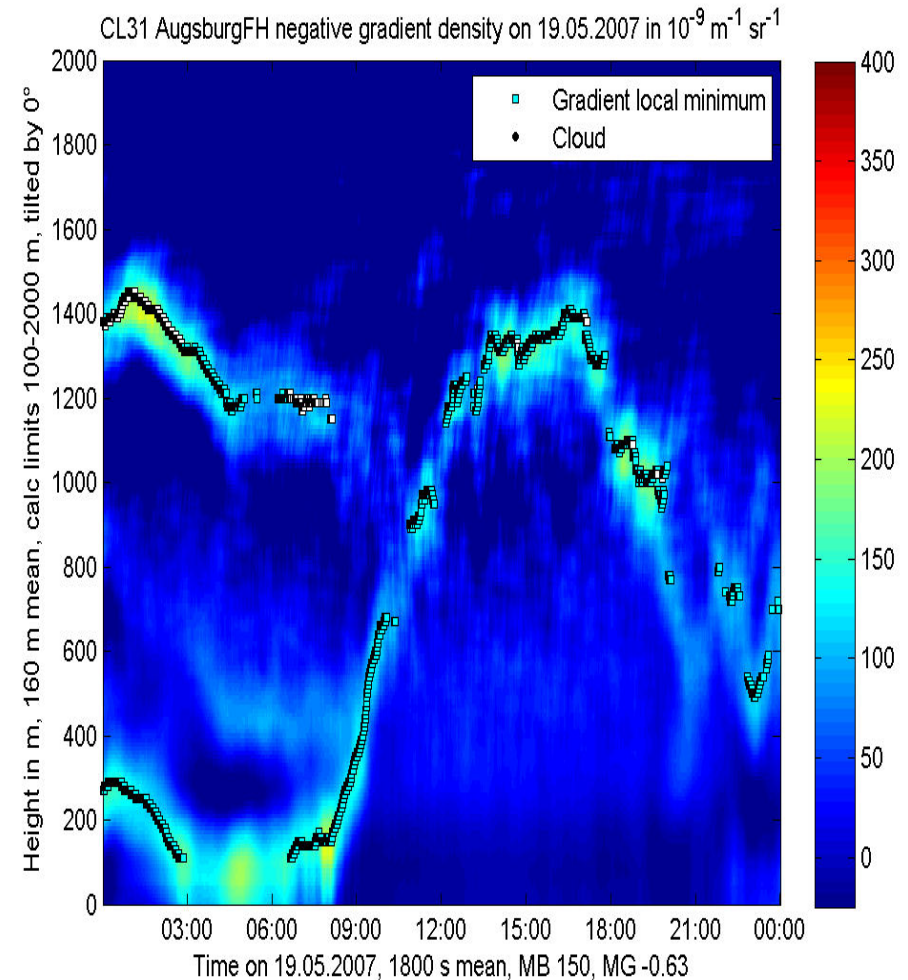
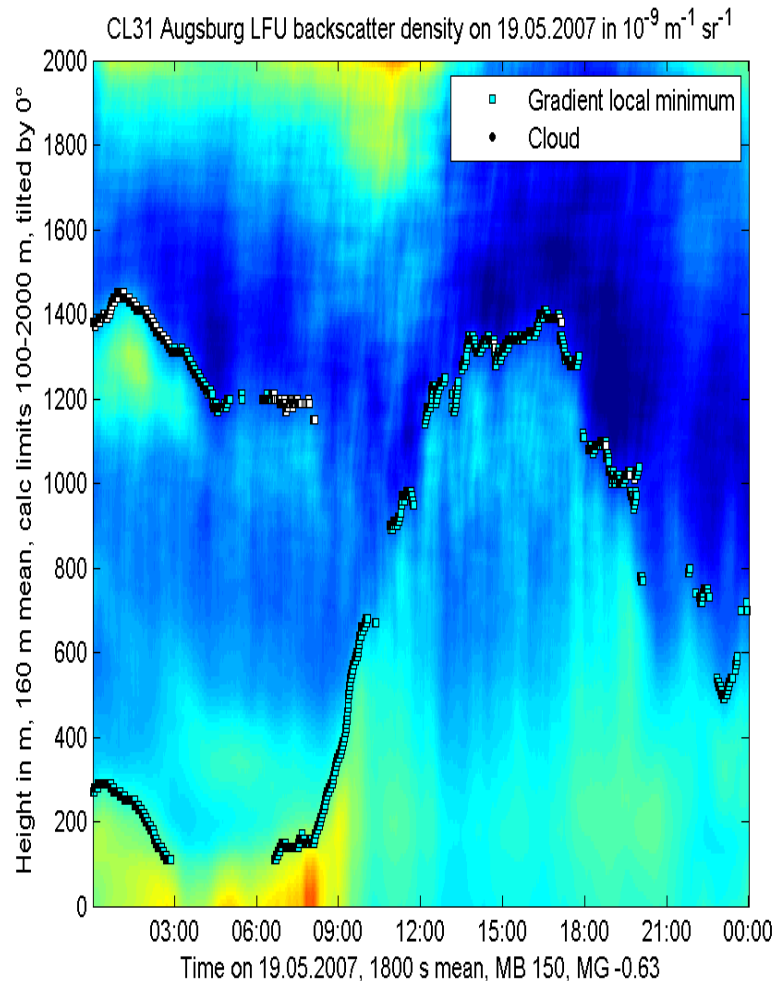
detection:

| | |
|-----------------------|--|
| travel time of signal | = height |
| backscatter intensity | = particle size and number distribution |
| Doppler-shift | = cannot be analyzed from ceilometer data (only from Wind-LIDAR: velocity component in line of sight) |

Sample plot ceilometer (convective BL at daytime)

optical backscatter intensity

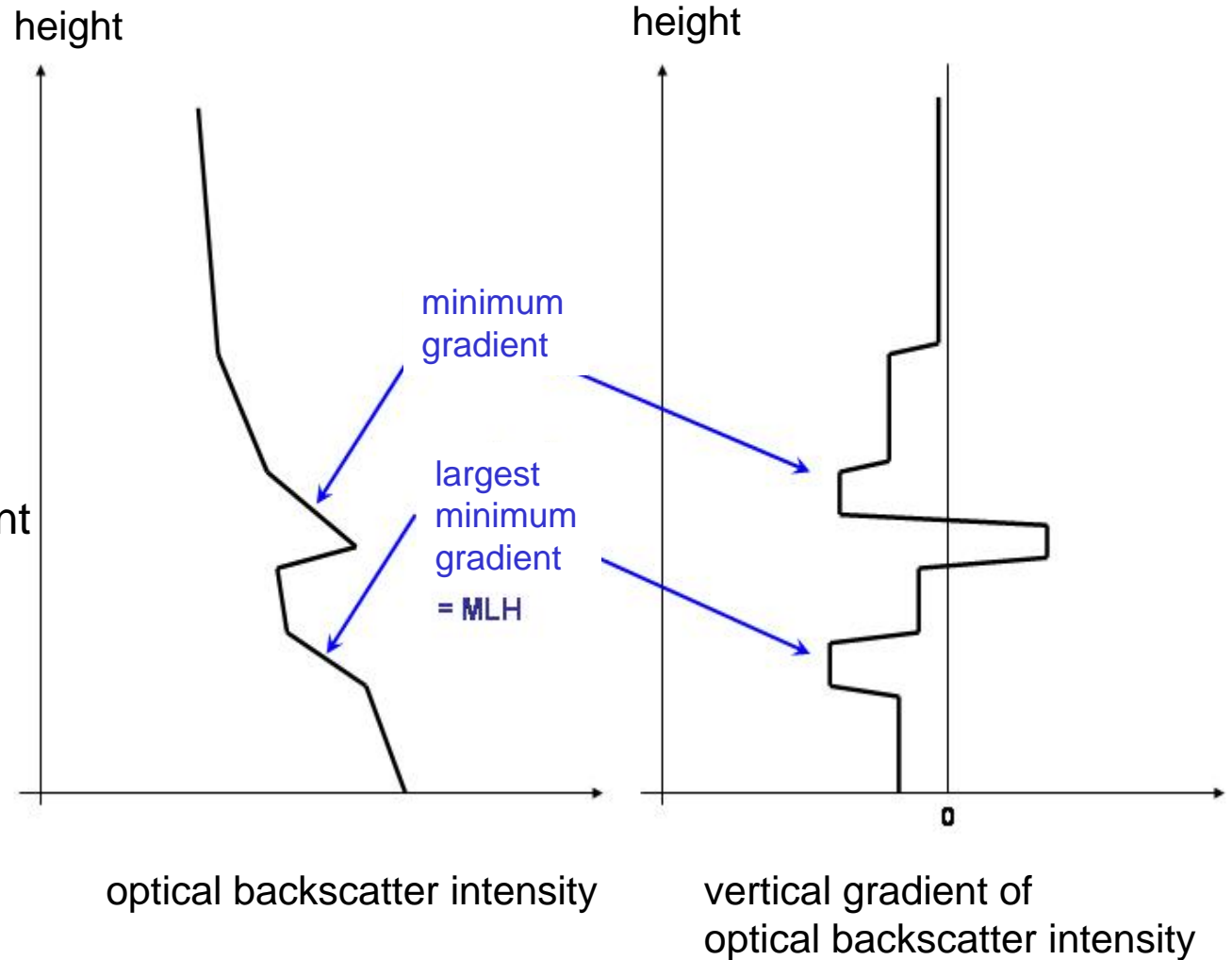
negative vertical gradient of optical backscatter intensity



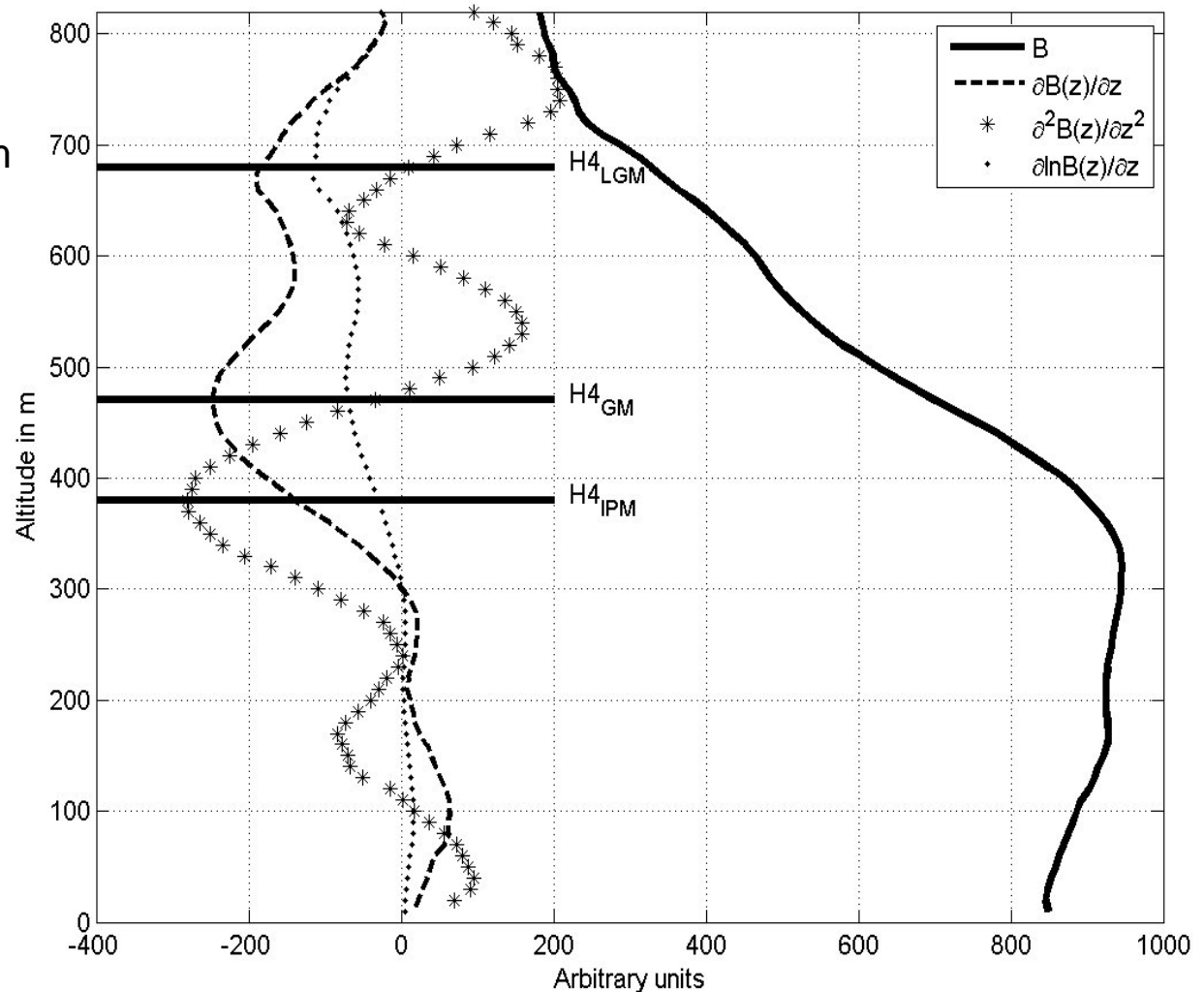
Algorithms to detect MLH from Ceilometer-Daten

criterion

minimal vertical gradient of backscatter intensity (the most negative gradient)



Different gradient methods (see Sicard et al. 2006, BLM 119, 135-157)



logarithmic gradient minimum

gradient minimum

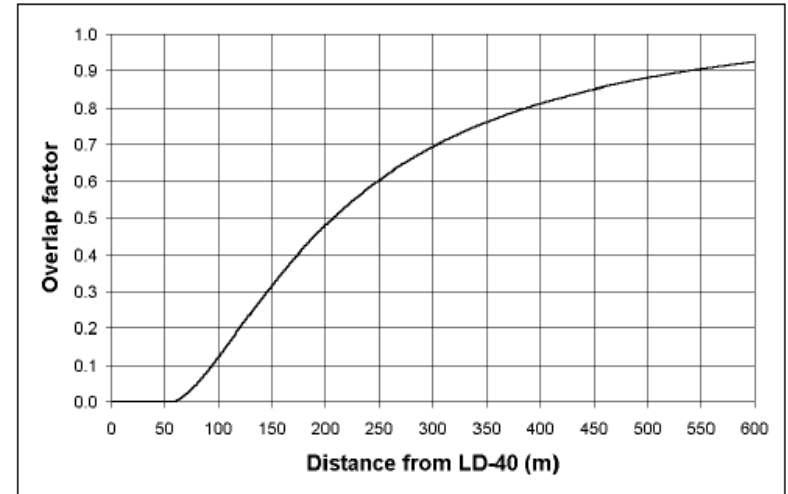
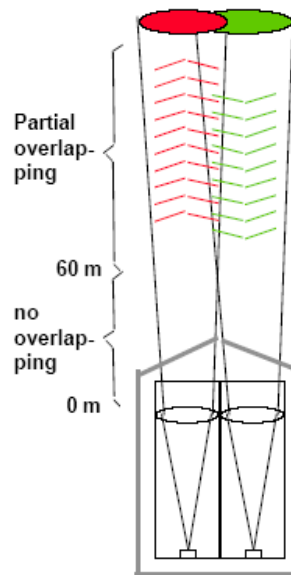
inflection point method
(minimum of 2nd derivative)

comparison of two different ceilometers

LD40

two optical axes

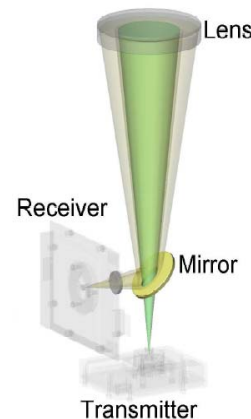
wave length: 855 nm
 height resolution: 7.5 m
 max. range: 13000 m



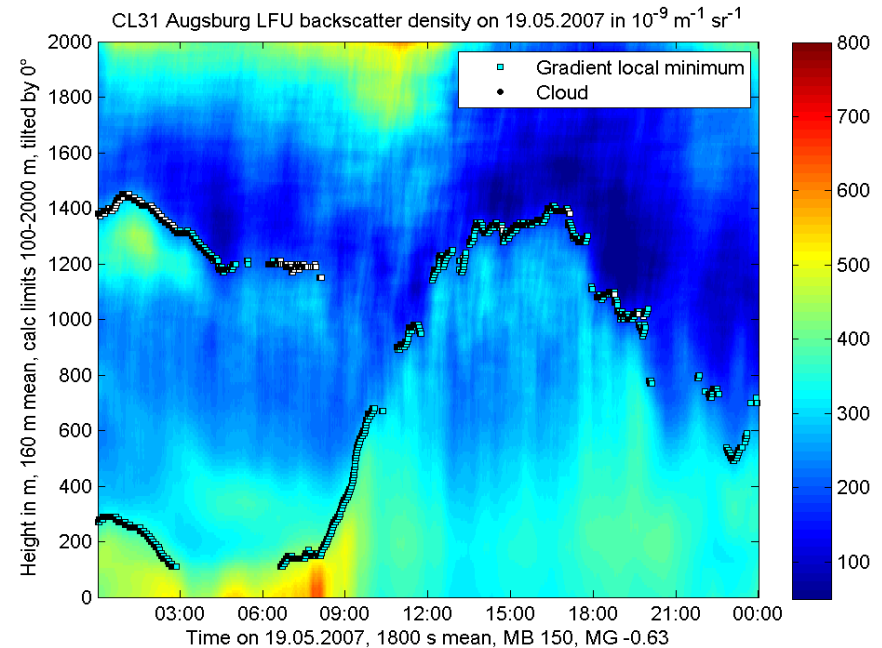
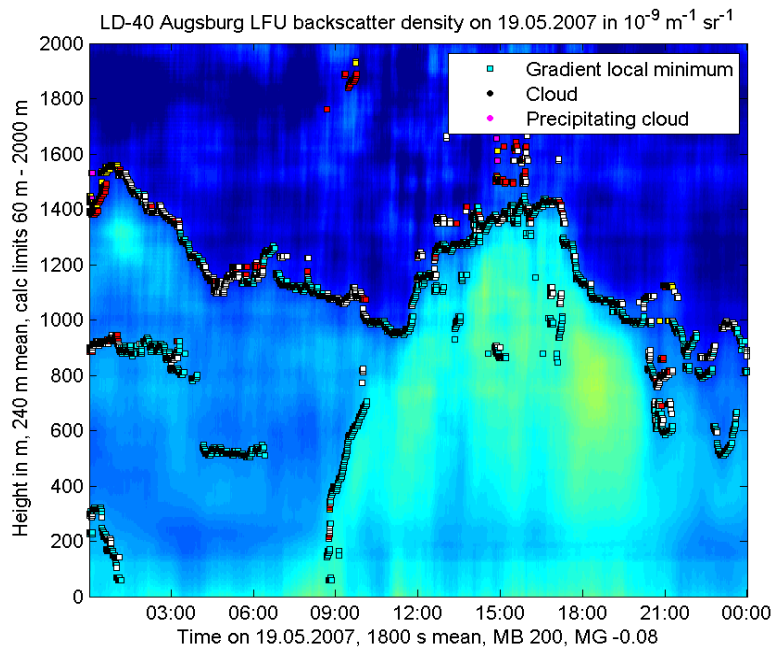
CL31

one optical axis

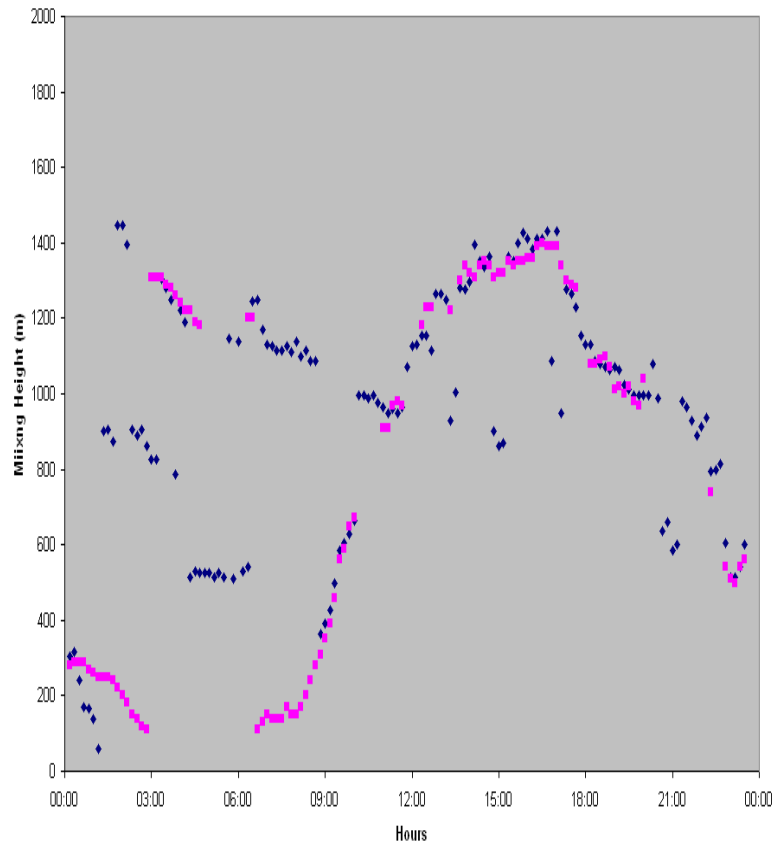
wave length: 905 nm
 height resolution: 5 m
 max. range: 7500 m



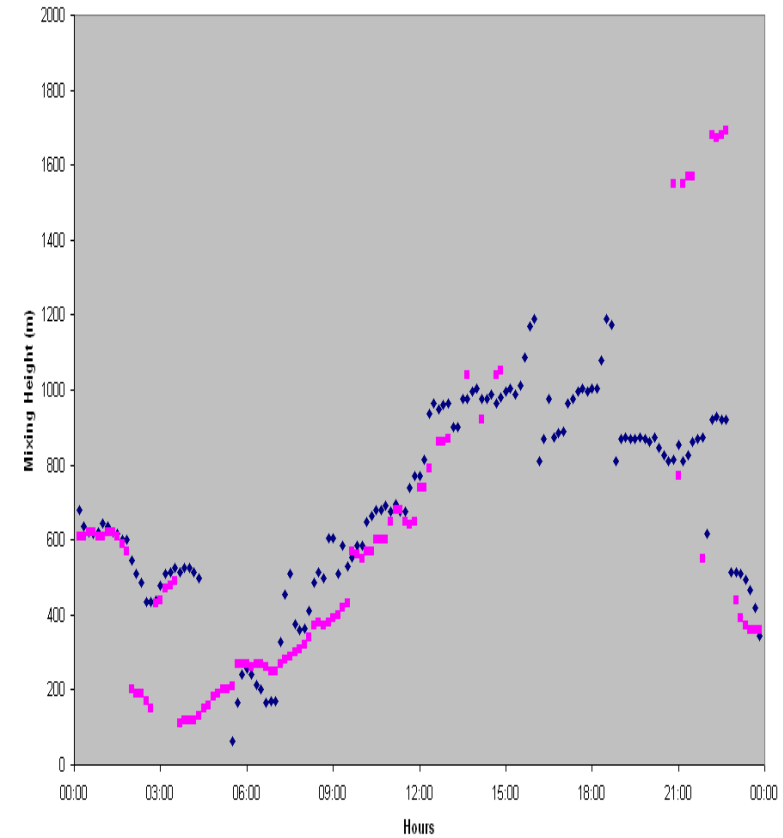
19 May 2007: ceilometer LD40 and CL31



comparison of MLH from LD40 and CL31 data



19 May 2007



20 May 2007

Comparison SODAR and Ceilometer

Measurement of the vertical structure of the boundary layer and mixing-layer height by remote sensing:

mobile surface-based acoustic and optical remote sensing yields information on:

→ thermal structure of the BL and turbulence intensity

(SODAR)

→ aerosol content of the BL

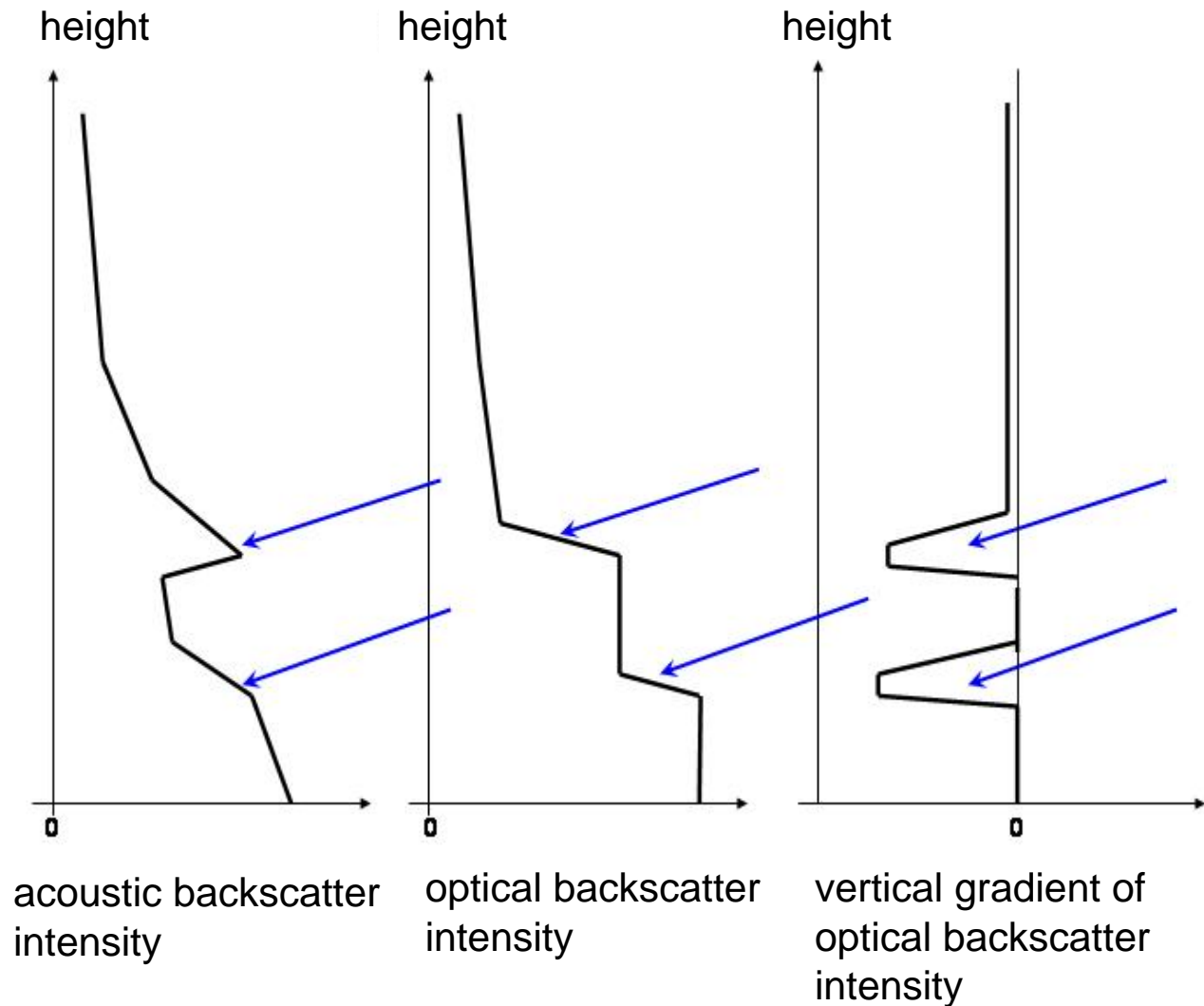
(Ceilometer)

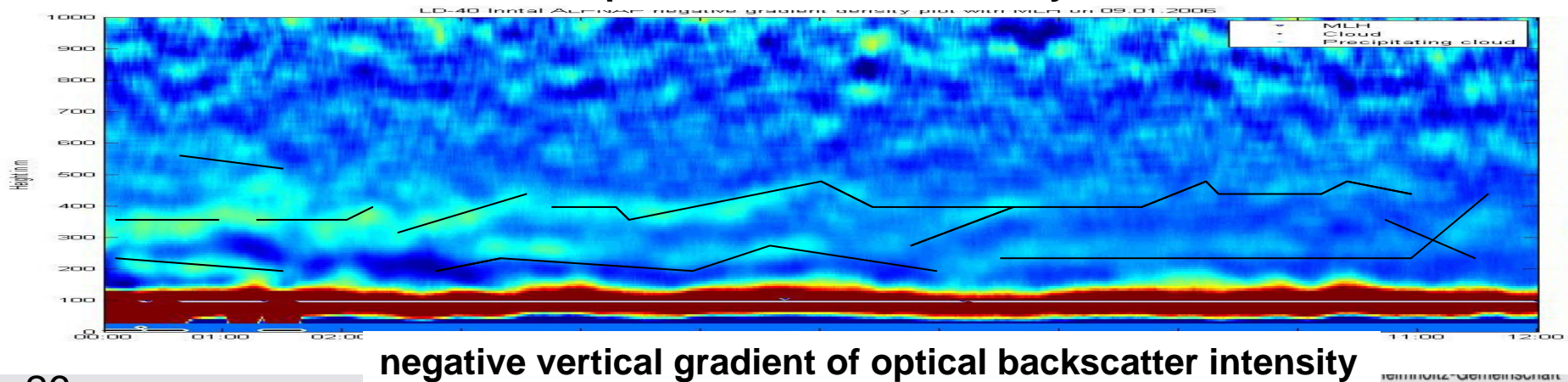
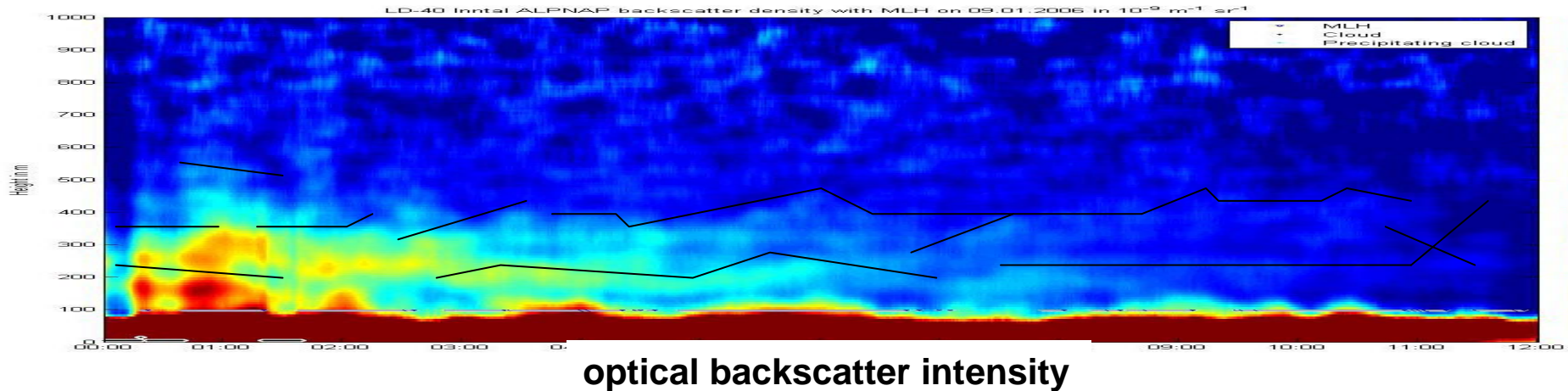
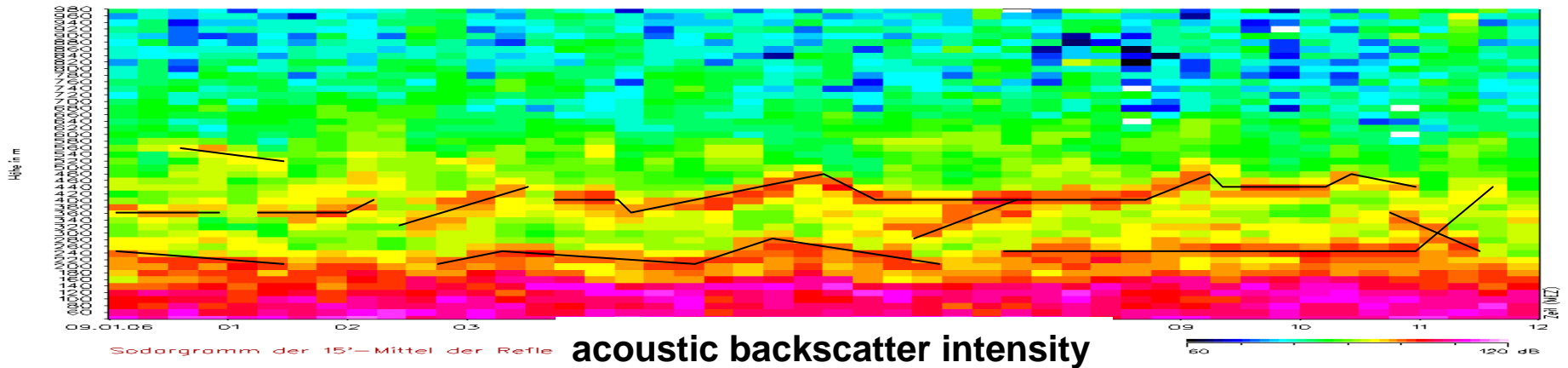


comparison of
algorithms

left: SODAR

middle and right:
ceilometer





Application examples for SODAR and Ceilometer

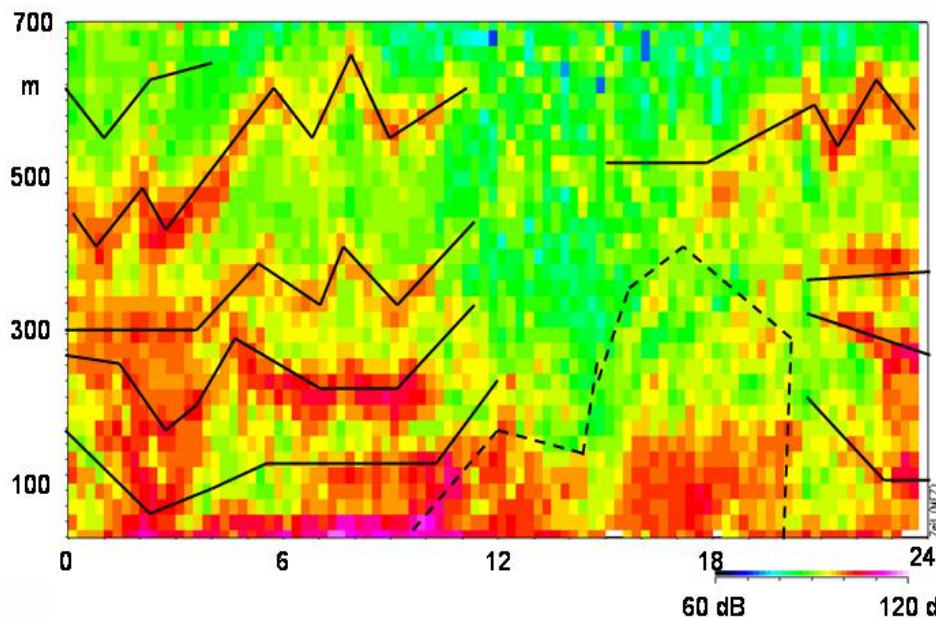
Example for the joint operation of a SODAR and a Ceilometer
winter in an Alpine valley (snow-covered)

(ALPNAP-Campaign in the Inn valley in winter 2005/06)

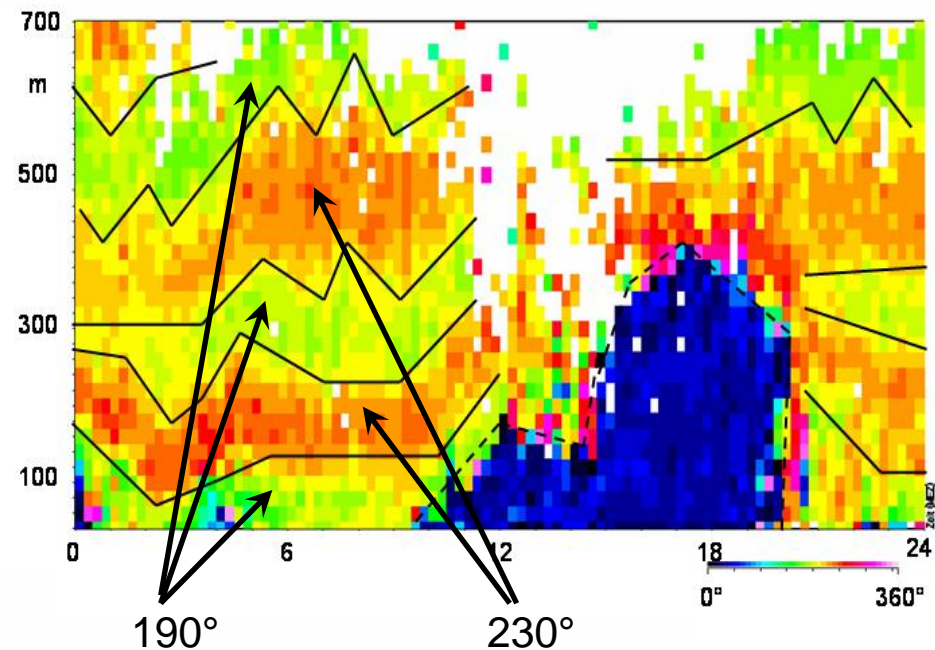
(ALPNAP was a project in the European Programme
INTERREG III B Alpine Space, ref. no. D/III/2.1/7)

SODAR measurements in a wintry Alpine valley

29 January 2006



backscatter intensity



wind direction

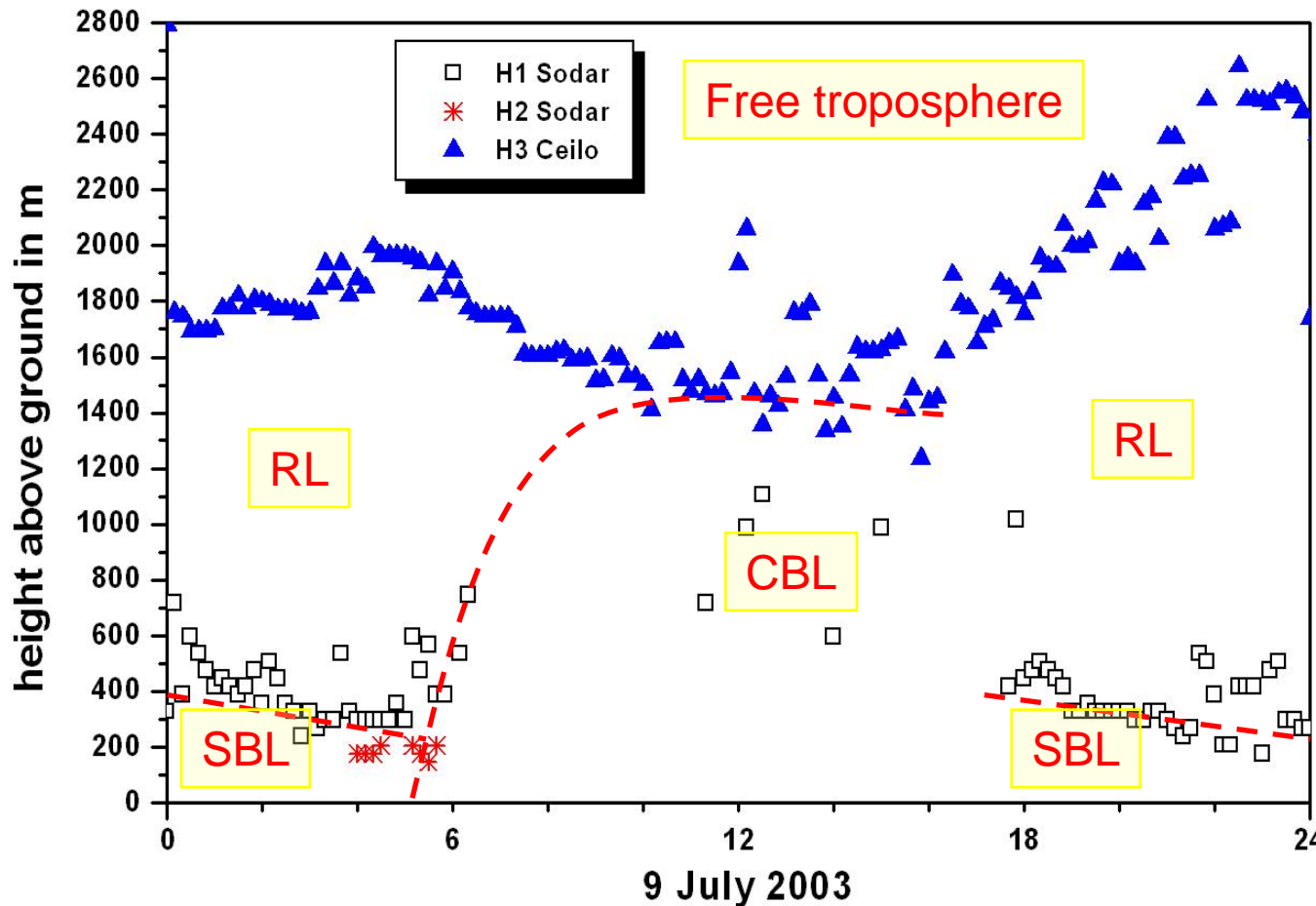
Example for the joint operation of a SODAR and a Ceilometer
summer 2003 Budapest (Hungary)

(ICAROS NET-Campaigns)



(ICAROS NET was a project within the European Research Framework
Programme FP5: IST-2000-29264)

Diurnal variation of mixing-layer height from SODAR and Ceilometer data (Budapest)



SBL:

stable boundary layer (usually at night and in winter)

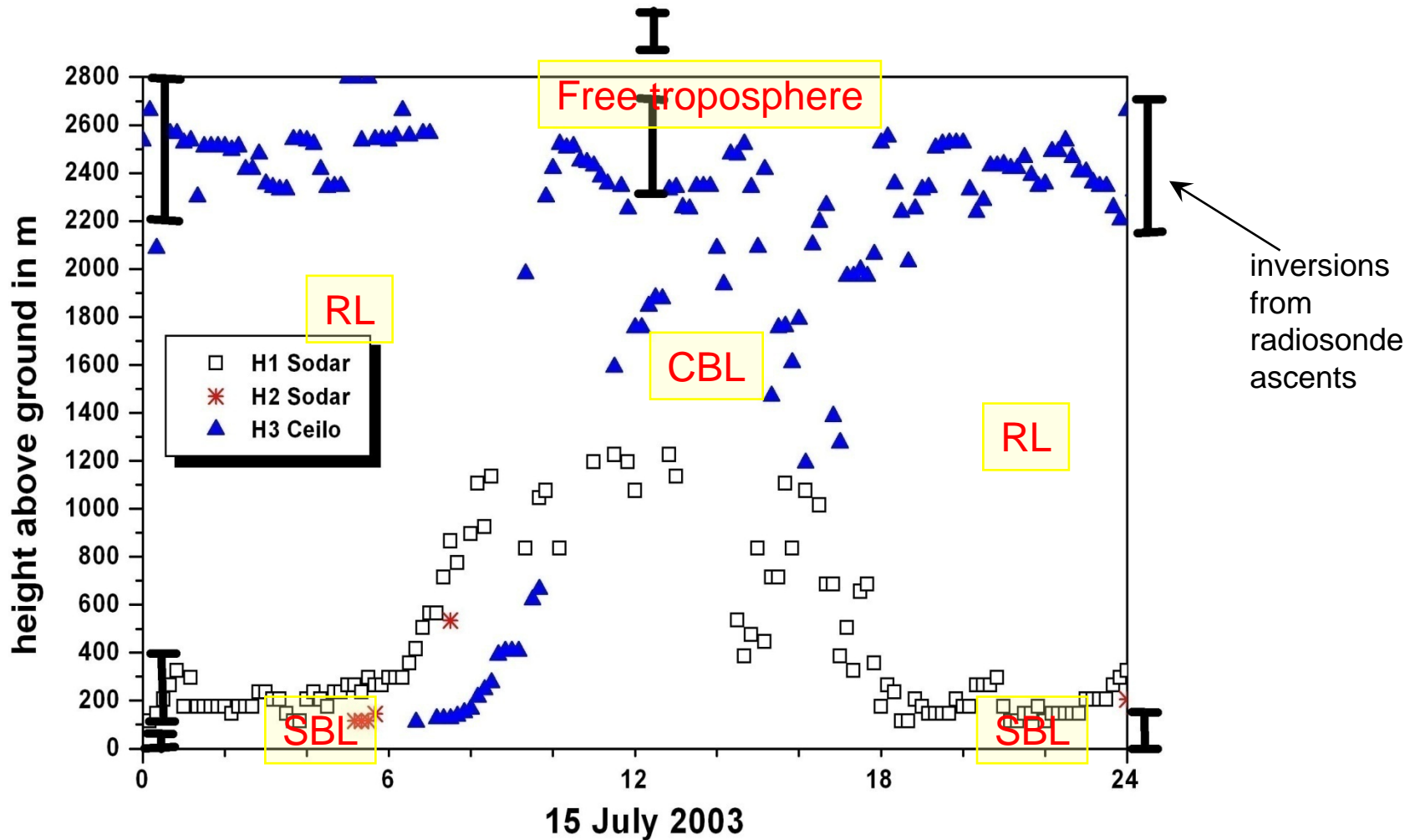
CBL:

convective boundary layer (usually at daytime due to strong insolation)

RL:

residual layer (usually at night-time)

Simultaneous operation SODAR-Ceilometer: examples for summer days



Emeis, S., K. Schäfer, 2006: Remote sensing methods to investigate boundary-layer structures relevant to air pollution in cities. *Bound.-Lay Meteorol.*, 121, 377-385,

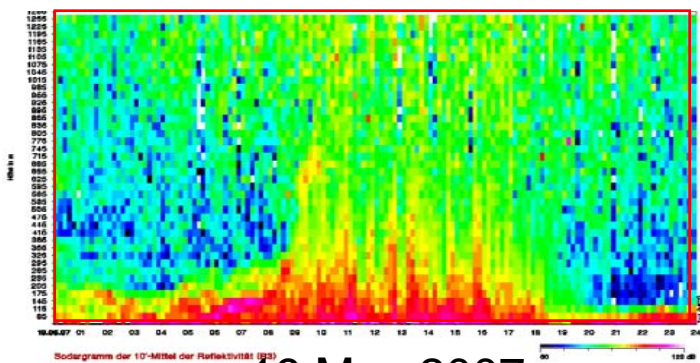
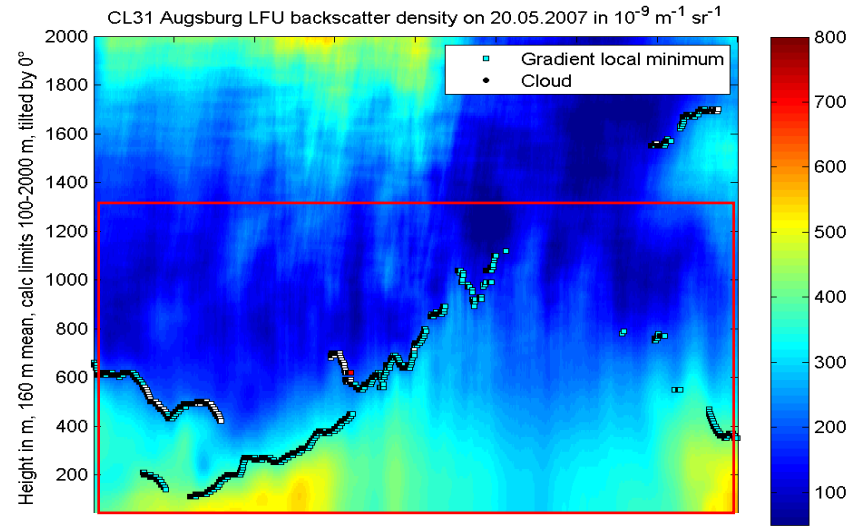
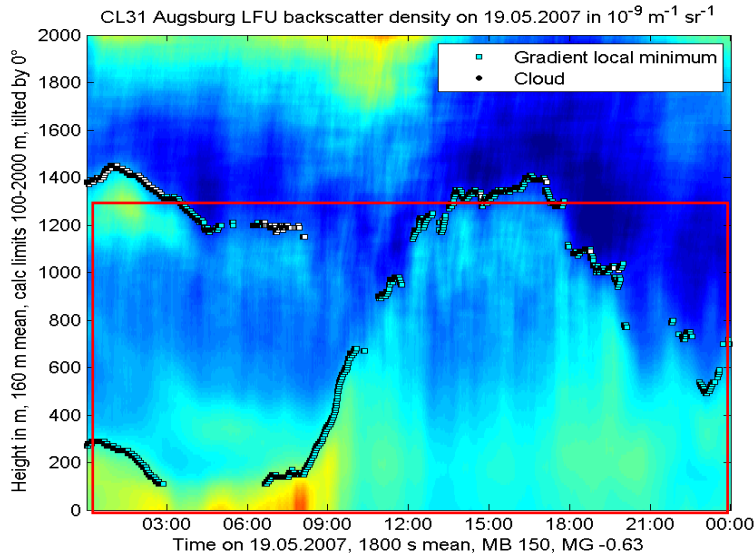
Example for the joint operation of a SODAR
and **two ceilometers (LD40 and CL31 of Vaisala)**

spatial variation of MLH over Augsburg (town with 250 000 inhabitants
in Germany)

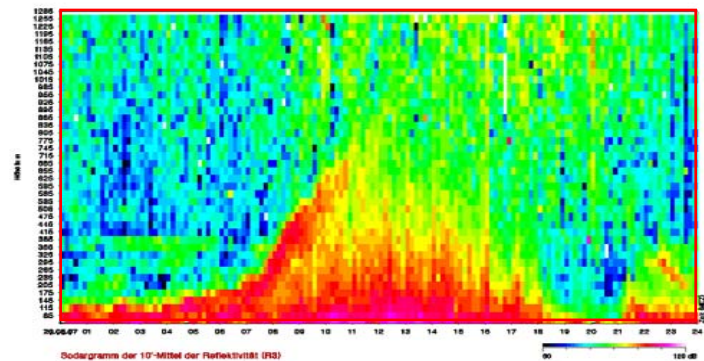
(measurement campaign in Augsburg since winter 2006/07)

(cooperation with University of Augsburg, Helmholtz Centre Munich
(health impact research), State Environmental Agency of Bavaria,
City of Augsburg)

comparison of optical (top) and acoustic (below) backscatter intensity

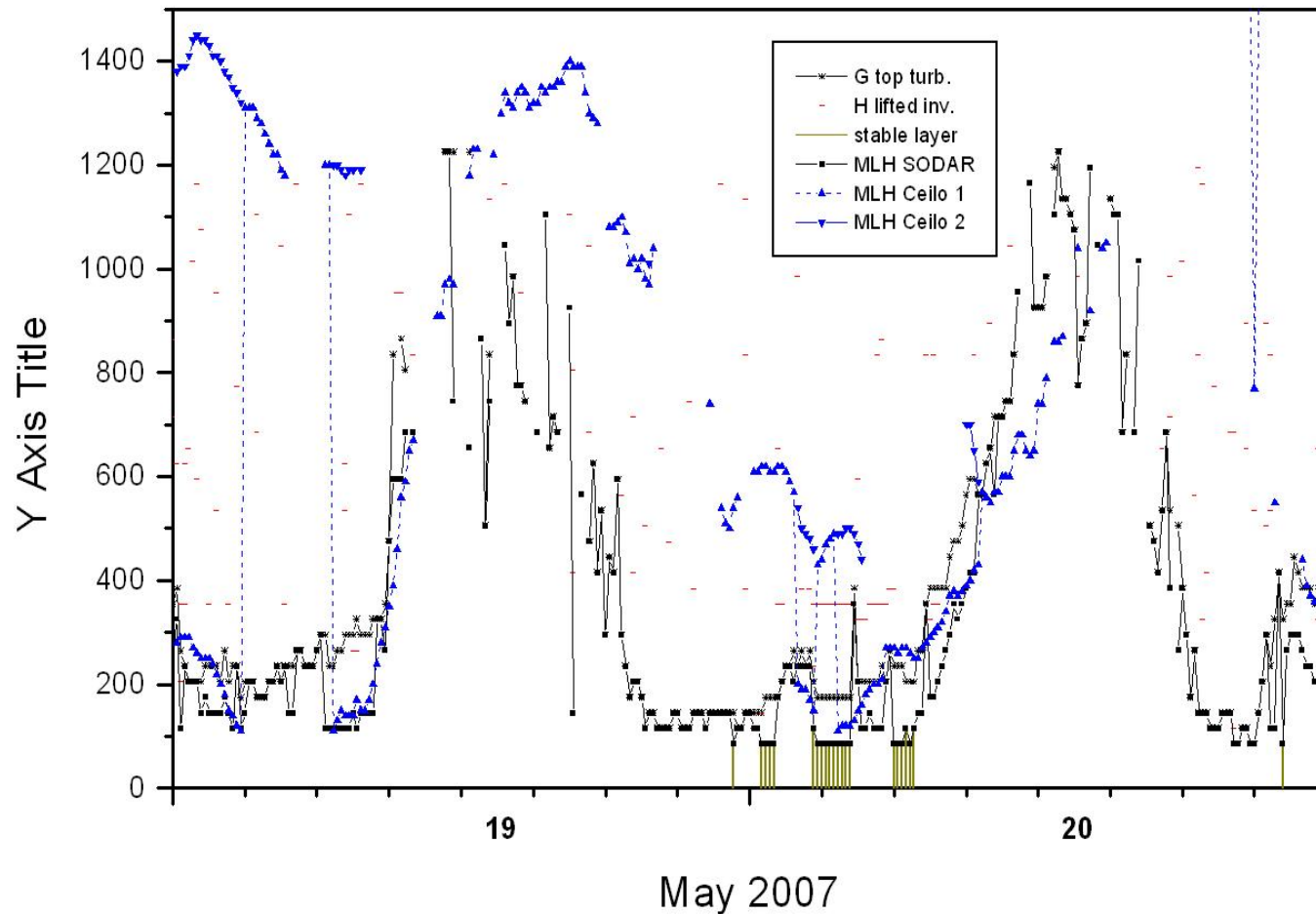


19 May 2007



20 May 2007

comparison of MLH from Sodar and CL31 data



RASS

principles of operation

examples

RASS (radio-acoustic remote sensing)

measures vertical temperature profiles

Bragg-RASS: windprofiler plus acoustic component

Doppler-RASS: SODAR plus electro-magnetic component

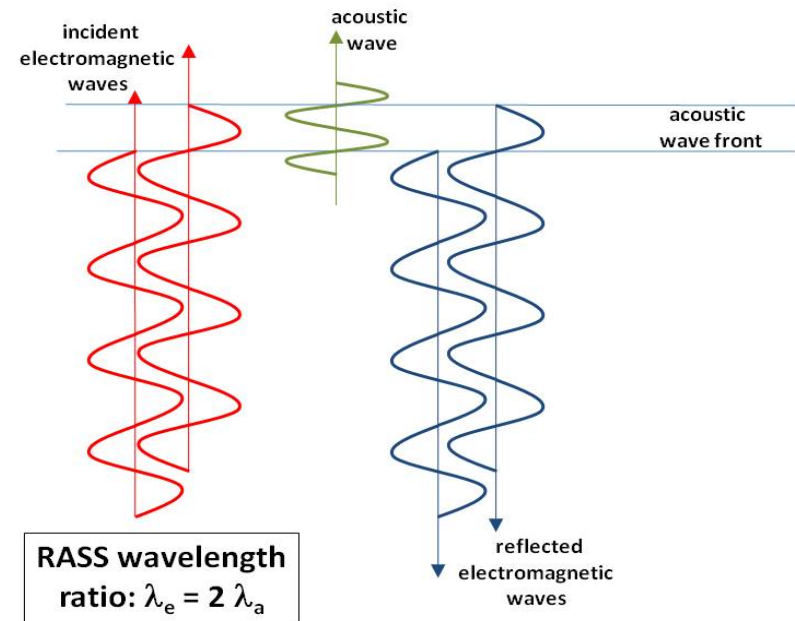
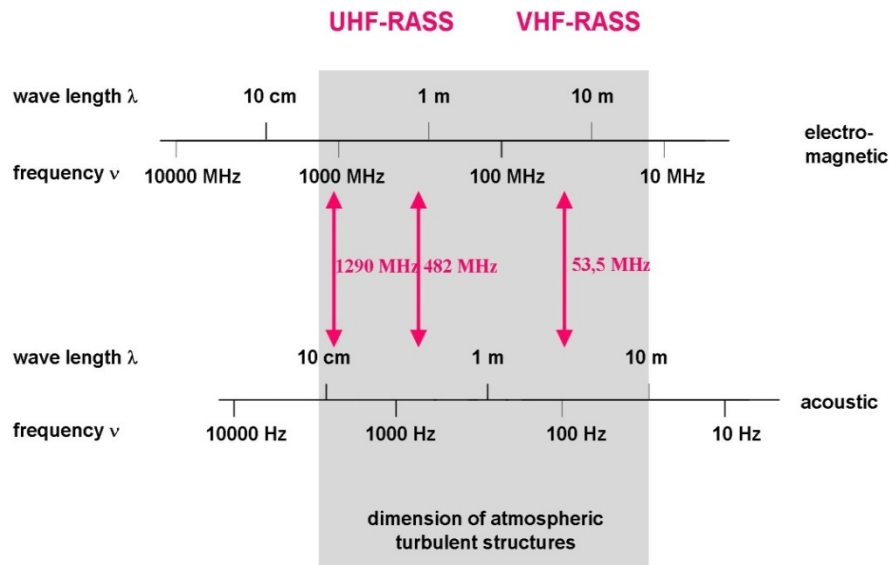
UHF RASS (boundary layer)

VHF RASS (troposphere)

RASS: frequencies

**Bragg condition:
acoustic wavelength = $\frac{1}{2}$ electro-magnetic wavelength**

electro-magnetic - acoustic frequency pairs for RASS devices





SODAR-RASS (Doppler-RASS)

(METEK)

acoustic frequ.: 1500 – 2200 Hz

radio frequ.: 474 MHz

resolution: 20 m

lowest

range gate: ca. 40 m

vertical range: 540 m



Bragg-RASS

acoustic frequ.: about 3000 Hz

radio frequ.: 1290 MHz

resolution: 50 m

lowest

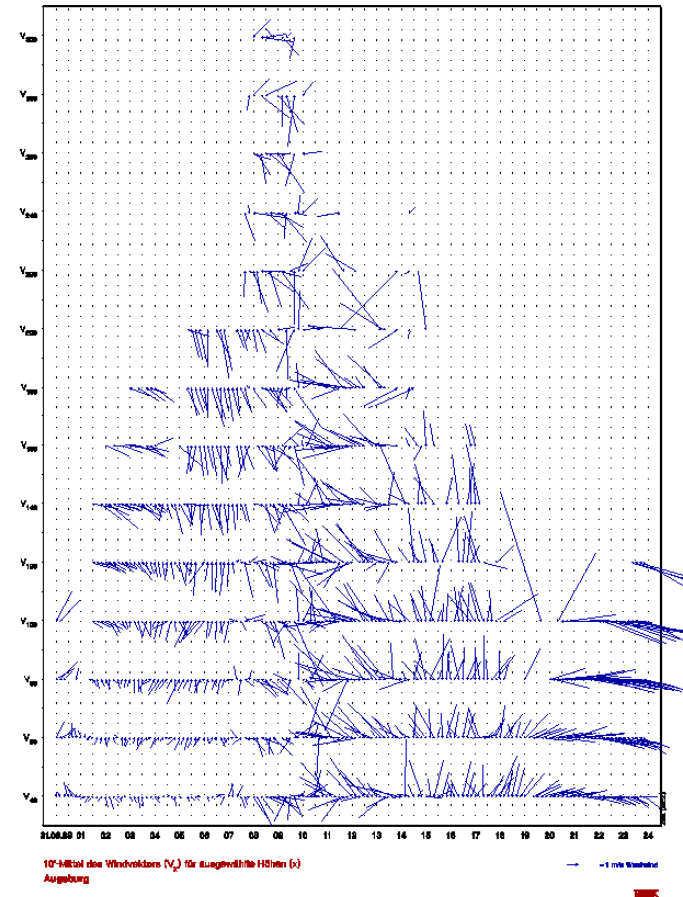
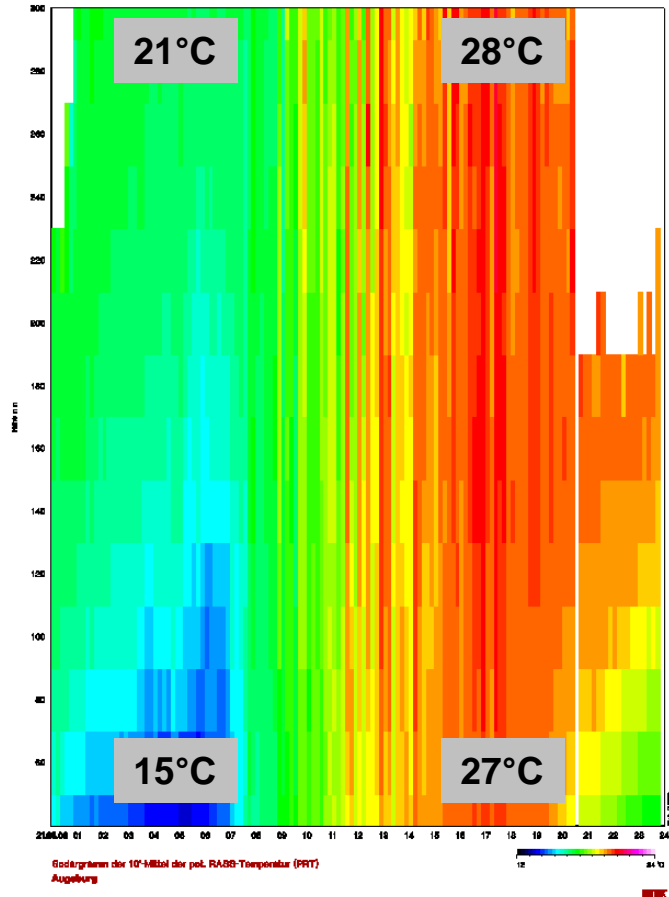
range gate: ca. 200 m

vertical range: 1000 m

temperature profile and dynamics

example RASS data: summer day
potential temperature (left), horizontal wind (right)

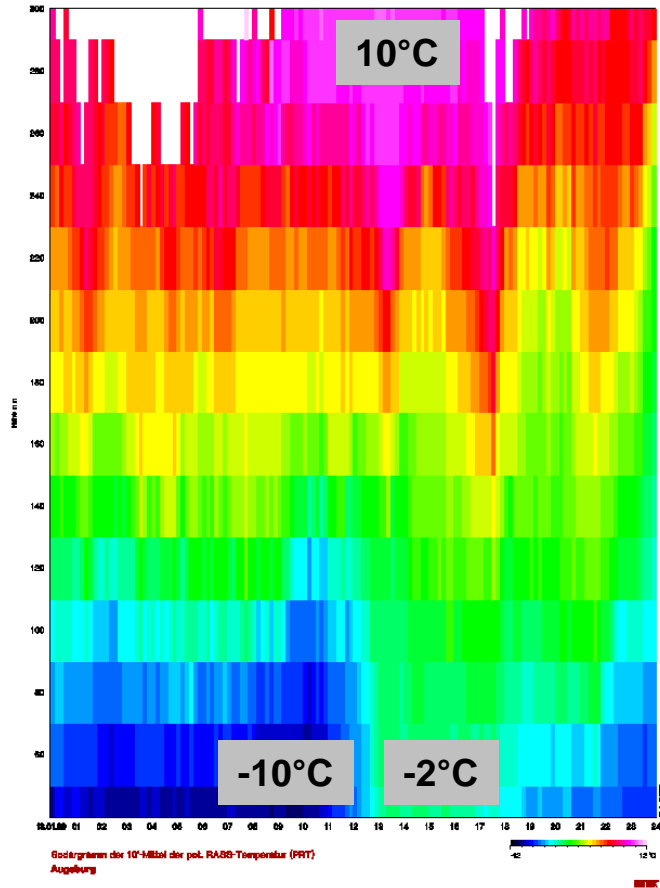
300 m



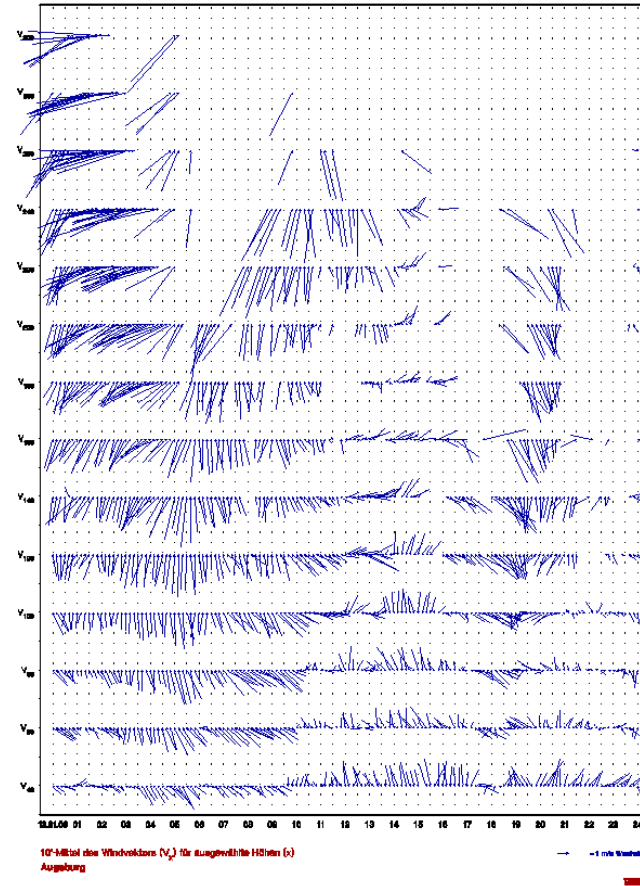
temperature profile and dynamics

example RASS data: winter day
potential temperature (left), horizontal wind (right)

300 m



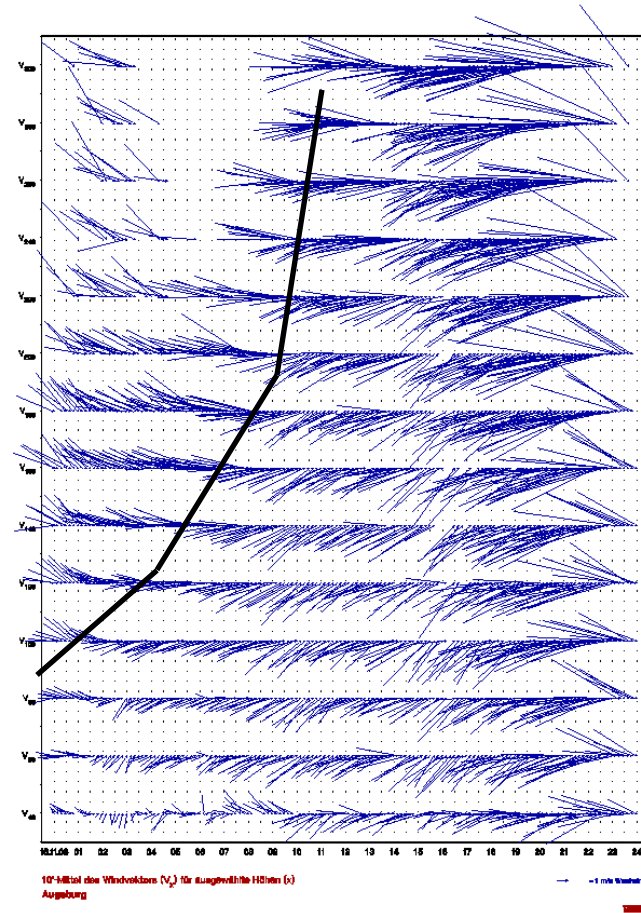
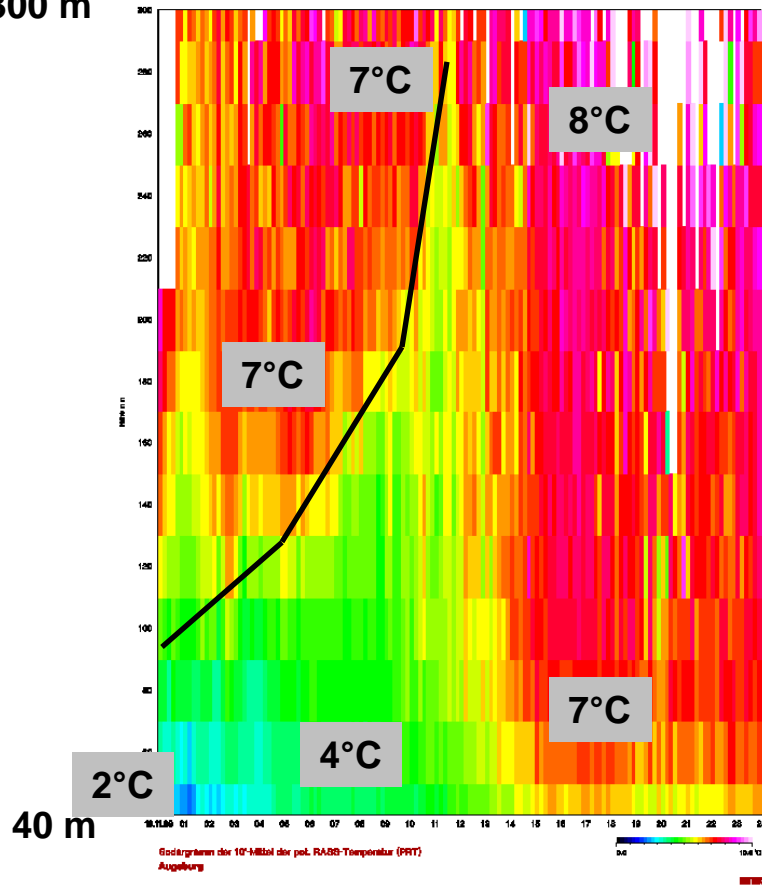
40 m



temperature profile and dynamics

example RASS data: inversion
potential temperature (left), horizontal wind (right)

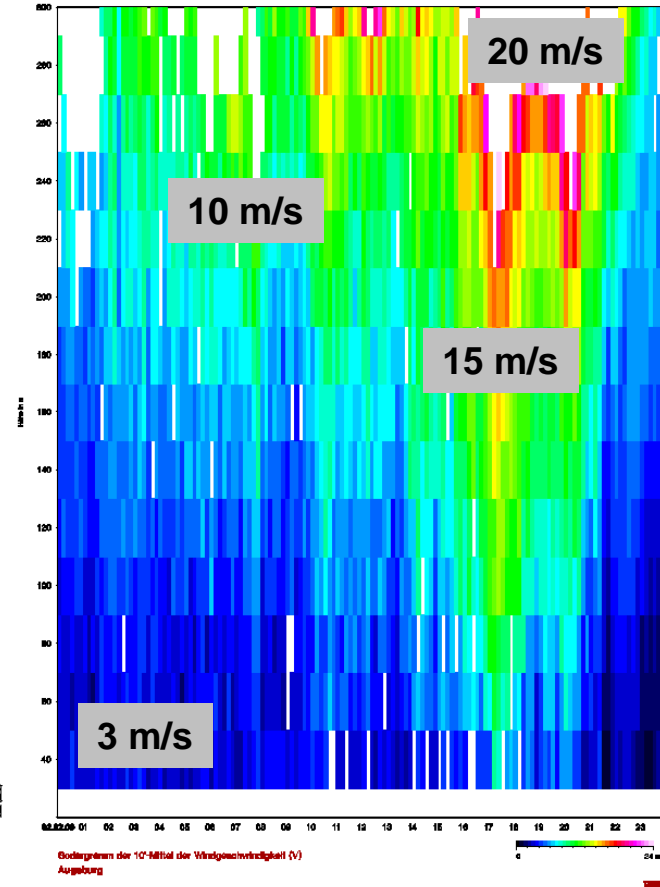
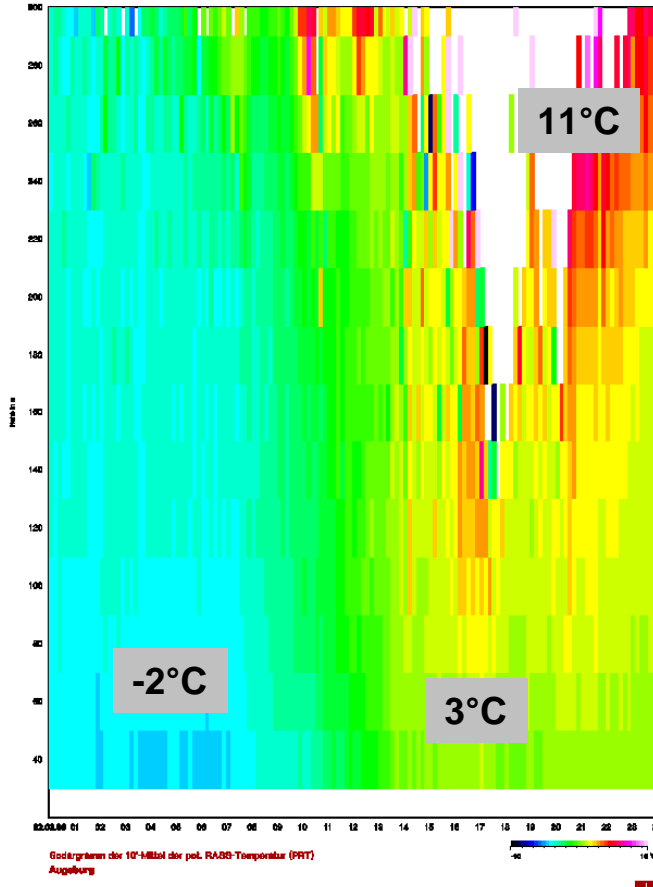
300 m



temperature profile and dynamics

example RASS data: inversion with strong wind shear
potential temperature (left), horizontal wind (right)

300 m

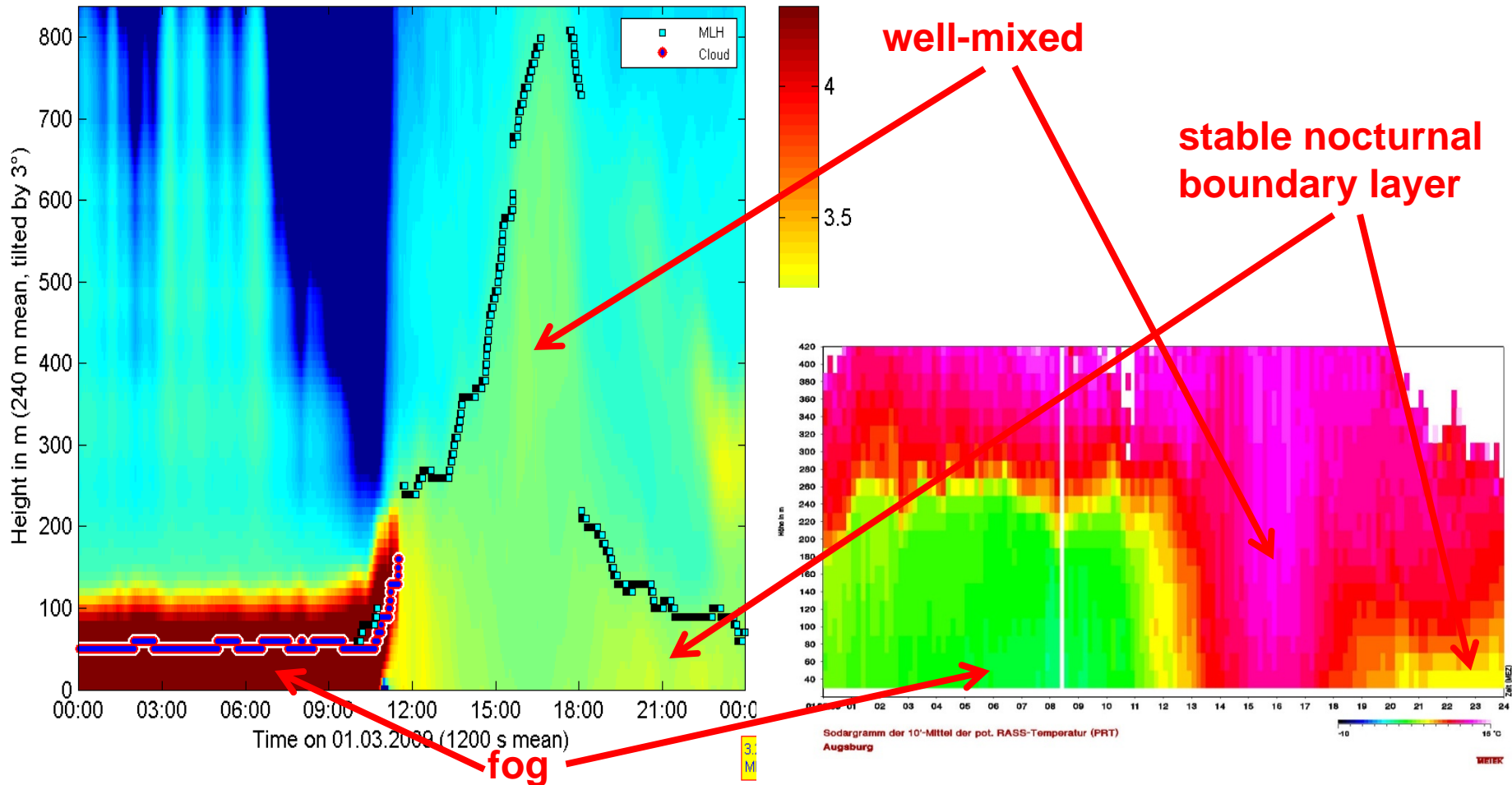


40 m

temperature profile and pollution

comparison of RASS data (potential temperature, right) with aerosol backscatter from a ceilometer (left)

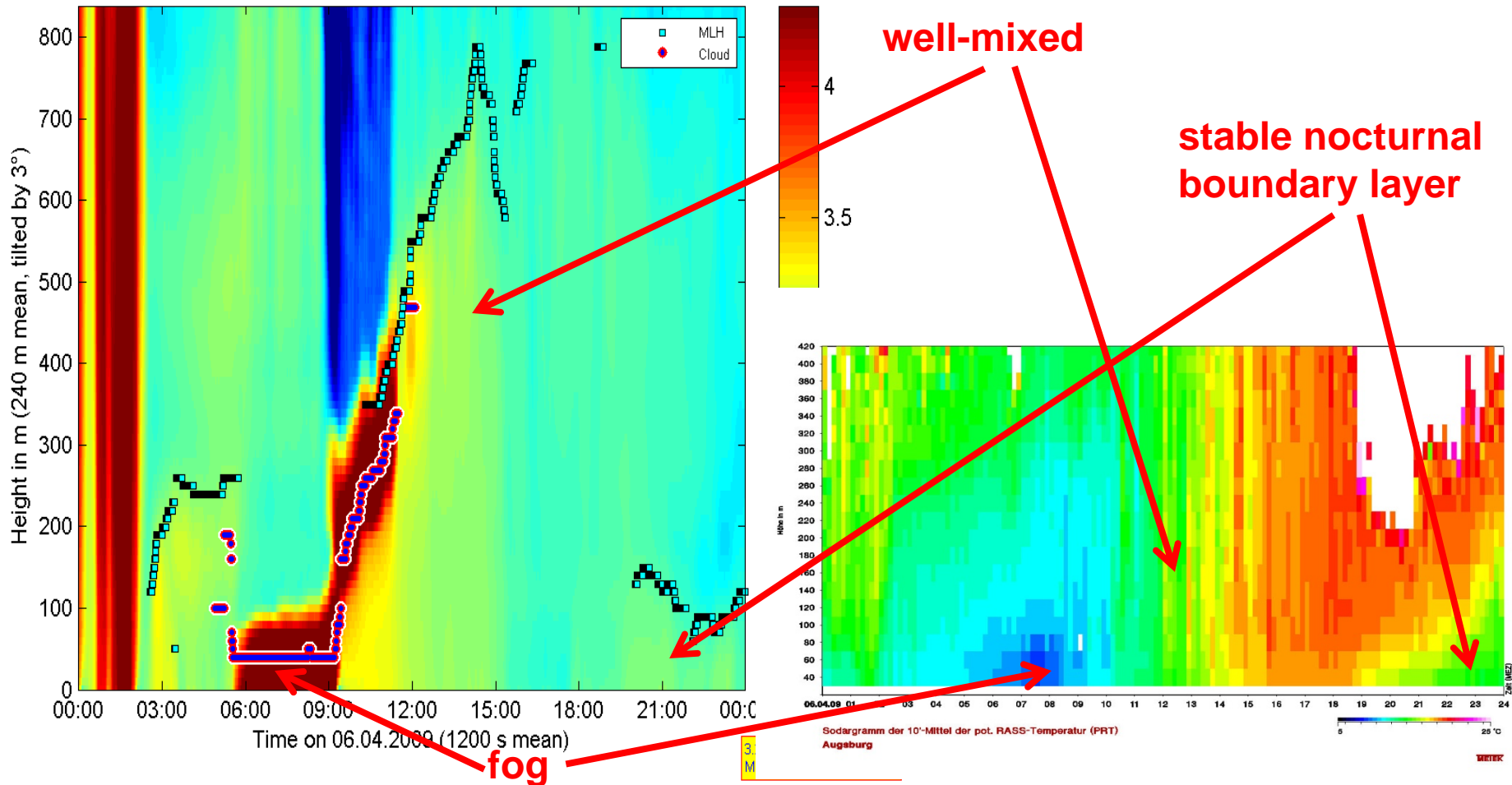
CL31 Augsburg AVA \log_{10} of backscatter with MLH on 01.03.2009 in $10^{-9} \text{ m}^{-1} \text{ sr}^{-1}$



temperature profile and pollution

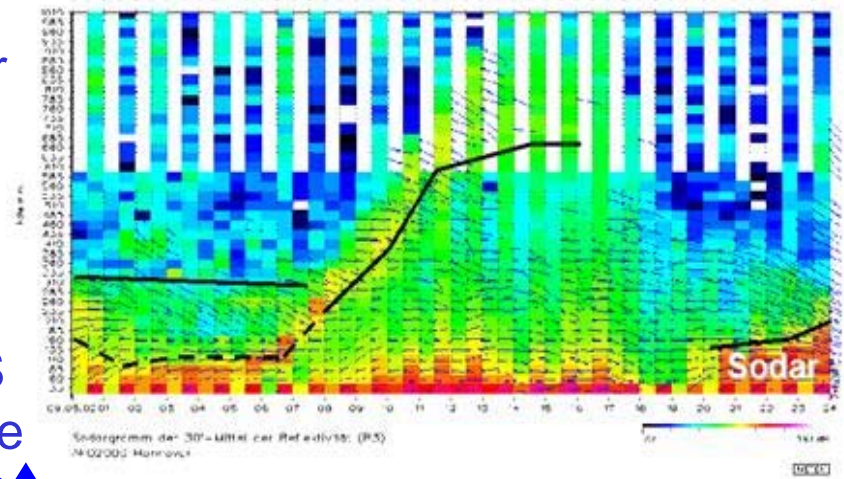
comparison of RASS data (potential temperature, right)
with aerosol backscatter from a ceilometer (left)

CL31 Augsburg AVA \log_{10} of backscatter with MLH on 06.04.2009 in $10^{-9} \text{ m}^{-1} \text{ sr}^{-1}$

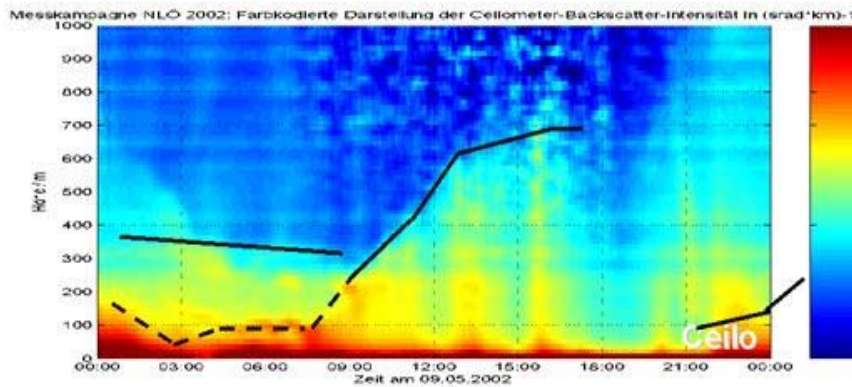


Comparison of MLH retrievals with three different remote sensing techniques

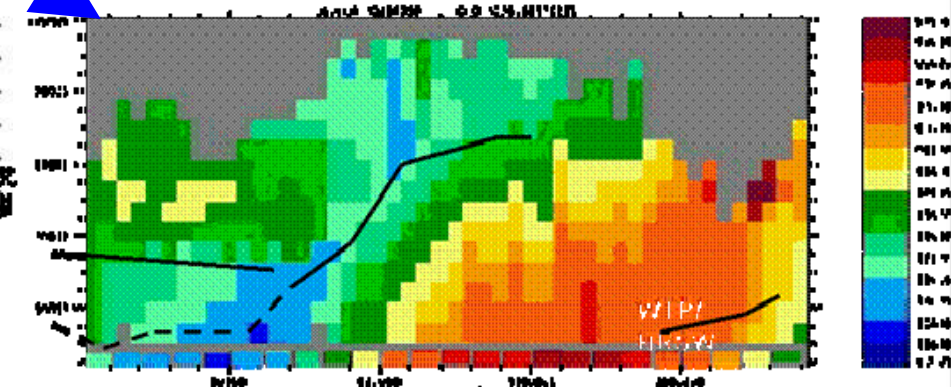
SODAR
acoustic backscatter



ceilometer
optical backscatter



RASS
temperature



Emeis, S., Chr. Münkel, S. Vogt, W.J. Müller, K. Schäfer, 2004: Atmospheric boundary-layer structure from simultaneous SODAR, RASS, and ceilometer measurements. Atmos. Environ., 38, 273-286.

Summary

Overview on methods using ground-based remote sensing for the derivation of the mixing-layer height

| method | short description |
|-------------------------------------|--|
| acoustic ARE method | analysis of acoustic received echo intensity profiles |
| “ HWS method | analysis of horizontal wind speed profiles |
| “ VWV method | analysis of vertical wind variance profiles |
| “ EARE method | analysis of acoustic backscatter intensity and vertical wind variance profiles (enhanced acoustic received echo method) |
| optical threshold method | detection of a given backscatter intensity threshold |
| “ gradient method | analysis of optical backscatter intensity profiles |
| “ idealised backscatter method | analysis of optical backscatter intensity profiles |
| “ wavelet method | analysis of optical backscatter intensity profiles |
| “ variance method | analysis of optical backscatter intensity profiles |
| acoustic / electro-magnetic | ARE method applied to sodar and wind profiler data |
| acoustic / optical | EARE method plus gradient method |
| electro-magnetic / electro-magnetic | combination of a sodar-RASS and a wind profiler RASS: analysis of the vertical temperature profile plus analysis of the electro-magnetic backscatter intensity profile |
| acoustic / in situ | ARE method plus in-situ surface flux measurement |

| | |
|-------------|---|
| RASS | analysis of the temperature profile from the measured speed of sound |
|-------------|---|

Conclusions:

RASS directly delivers temperature profiles, MLH, inversions, and stable layers can easily be detected, wind profiles are additionally available.

Does not work properly with high wind speeds.

SODAR detects temperature fluctuations and gradients, but no absolute temperature. Inversions and stable layers can indirectly be inferred with a MLH algorithm.

Does not work properly with perfectly neutral stratification, with very high wind speeds, and during stronger precipitation events.

Ceilometer detects aerosol distribution and water droplets. It has to be assumed that the aerosol follows the thermal structure of the atmosphere. Inversions and MLH can indirectly be inferred with a MLH algorithm.

Does not work properly in extreme clear (aerosol-free) air and during precipitation events and fog.

Literature

Asimakopoulos, D.N., C.G. Helmis, J. Michopoulos, 2004: Evaluation of SODAR methods for the determination of the atmospheric boundary layer mixing height. - Meteor. Atmos. Phys. 85, 85–92.

Beyrich, F., 1997: Mixing height estimation from sodar data – a critical discussion. - Atmos. Environ. 31, 3941–3953.

Ceilometer:

Schäfer, K., S.M. Emeis, A. Rauch, C. Münkel, S. Vogt, 2004: Determination of mixing-layer heights from ceilometer data. In: Remote Sensing of Clouds and the Atmosphere IX. Schäfer, K., A. Comeron, M. Carleer, R.H. Picard, N. Sifakis (Eds.), Proc. SPIE, Bellingham, WA, USA, Vol. 5571, 248–259.

Sicard, M., C. Pérez, F. Rocabenbosch, J.M. Baldasano, D. García-Vizcaino, 2006: Mixed-Layer Depth Determination in the Barcelona Coastal Area From Regular Lidar Measurements: Methods, Results and Limitations. - Bound.-Lay. Meteor. 119, 135–157.

RASS:

Engelbart, D.A.M., J. Bange, 2002: Determination of boundary-layer parameters using wind profiler/RASS and sodar/RASS in the frame of the LITFASS project. Theor. Appl. Climatol. 73, 53–65.

Emeis, S., K. Schäfer, C. Münkel, 2009: Observation of the structure of the urban boundary layer with different ceilometers and validation by RASS data. Meteorol. Z., 18, 149-154. (Open access, freely available from <http://dx.doi.org/10.1127/0941-2948/2009/0365>)

Reviews:

Emeis, S., K. Schäfer, C. Münkel, 2008: Surface-based remote sensing of the mixing-layer height – a review. - Meteorol. Z., 17, 621-630. (Open access, freely available from <http://dx.doi.org/10.1127/0941-2948/2008/0312>)

Emeis, S., M. Harris, R.M. Banta, 2007: Boundary-layer anemometry by optical remote sensing for wind energy applications. - Meteorol. Z., 16, 337-347.